

Rapid emergence of overmassive black holes in the early Universe

Sunmyon Chon^{1*}, Shingo Hirano^{2,3†}, Tomoaki Ishiyama^{4†},
Seok-Jun Chang¹, Volker Springel^{1†}

¹Max-Planck-Institut für Astrophysik, Karl-Schwarzschild-Str. 1,
Garching, D-85741, Garching bei München, Germany.

²Department of Applied Physics, Faculty of Engineering, Kanagawa University, 3-27-1 Rokukakubashi, Kanagawa, Yokohama, Kanagawa, 221-0802, Japan.

³Department of Astronomy, School of Science, University of Tokyo,
7-3-1 Hongo, Bunkyo, Tokyo, 113-0033, Japan.

⁴Digital Transformation Enhancement Council, Chiba University, 1-33, Yayoi-cho, Inage-ku, Chiba, 263-8522, Japan.

*Corresponding author(s). E-mail(s):
sunmyon@MPA-Garching.MPG.DE;

Contributing authors: shingo-hirano@kanagawa-u.ac.jp;
ishiyama@chiba-u.jp; sjchang@MPA-Garching.MPG.DE;
v.springel@MPA-Garching.MPG.DE;

†These authors contributed equally to this work.

Abstract

The origin of supermassive black holes (SMBHs) remains a long-standing problem in astrophysics. Recent JWST observations reveal an unexpectedly abundant population of overmassive black holes at $z > 4-6$, where the BH masses lie far above local scaling relations and not reproduced by current cosmological models. How such overmassive black holes form and rapidly grow within young galaxies has remained unclear. Here we present fully cosmological radiation-hydrodynamic simulations that, for the first time, self-consistently follow the birth, early growth, and emergent observable signatures of SMBHs in proto-cluster environments. We find that heavy seeds of order $10^6 M_\odot$ naturally form, exceeding typical theoretical expectations by an order of magnitude. These seeds rapidly develop dense, optically thick disks whose strong electron scattering produces broad H α

emission comparable to that seen in little red dots (LRDs). Sustained super-Eddington accretion then drives fast growth to $\sim 3 \times 10^7 M_\odot$ by $z \simeq 8$. These results provide a unified physical scenario in which LRDs correspond to a short-lived, enshrouded phase of heavy-seed formation, naturally evolving into the overmassive quasars detected by JWST and ultimately the progenitors of today's SMBHs.

Supermassive black holes (SMBHs) are known to exist less than a billion years after the Big Bang, yet how they were seeded and grew remains unclear. Recent *James Webb Space Telescope* (JWST) observations have revealed compact, red sources at $z > 4\text{--}6$, the so-called little red dots (LRDs), whose inferred black-hole (BH) masses exceed local scaling relations [1–5]. Their spectra point to rapid BH growth in dense, obscured environments during early galaxy assembly [6–10], consistent with recent theoretical predictions [11–13]. However, proposed pathways such as direct-collapse BHs or Population III remnants rely on idealized conditions and have not been followed self-consistently in cosmological simulations [14, 15]. Here we show that heavy BH seeds naturally form in overdense proto-cluster regions exposed to intense far-ultraviolet (FUV) radiation, where the collapse of supermassive stars produces $\sim 10^6 M_\odot$ seeds that undergo brief super-Eddington growth. These systems reproduce the Balmer features and red continua seen in LRDs and rapidly grow into overmassive BHs by $z \sim 8$. Our results provide a unified pathway linking the birth of massive seeds, their short-lived obscured growth phases, and the overmassive BHs discovered by JWST, offering a cosmological explanation for their abundance and properties.

Rapid emergence of overmassive BHs

Our cosmological radiation–hydrodynamic simulations naturally produce massive BH seeds that grow into overmassive ($\gtrsim 10^7 M_\odot$) BHs by $z \sim 10$. This rapid growth occurs in overdense proto-cluster regions exposed to intense FUV radiation from nearby star-forming galaxies, where the radiation suppresses early star formation. We follow the collapse of one such halo using three-dimensional radiation-hydrodynamic simulations performed with the moving-mesh code AREPO [16] (see Methods). The halo—identified in Ishiyama and Hirano [17] as a promising heavy-seed site—is located ~ 10 kpc from a luminous neighbour that provides the strong FUV flux needed to form heavy seeds (Extended Data Fig. 1). As a result, the halo accumulates a large gas reservoir before collapsing at $z \simeq 14$ (Fig. 1a,b). Once collapse sets in, the central protostars grow rapidly, reaching $5\text{--}9 \times 10^5 M_\odot$, well above the canonical $\sim 10^5 M_\odot$ predicted by standard direct-collapse models [18–22]. The unusually deep potential well of the host halo (virial temperature $\sim 4 \times 10^4$ K; Extended Data Fig. 2) enables ionized gas to remain gravitationally bound and sustain the high accretion rates needed to form such massive seeds. Multiple seed-forming sites emerge within the same overdense environment, indicating that heavy-seed formation can naturally occur in proto-cluster regions.

These massive seeds do not remain static; each heavy seed subsequently experiences a brief but intense phase of super-Eddington accretion (Fig. 1f). Immediately

after collapse, a dense and optically thick envelope develops around the nascent BH, efficiently feeding the accretion disk. Radiation trapping becomes important: photons are advected inward faster than they can diffuse outward, enabling accretion rates several to a few tens of times the Eddington limit for less than a million years [23–25]. The inflowing gas is supplied from the circum-BH disk, inside which the gas loses angular momentum through gravitational torques. This sustains rapid growth until the reservoir is exhausted, where the BHs reach several $\times 10^6 M_\odot$ shortly after formation. The accretion rate then gradually decreases to 0.1–1 times the Eddington limit as the gas supply dwindles, allowing the BHs to grow to $\gtrsim 10^7 M_\odot$ by redshift $z \simeq 10$.

At $z \simeq 10$, the accretion rate sharply declines to below 1% of the Eddington limit. As the BHs pass through the central region of the massive neighboring halo, their envelope gas is stripped by the surrounding hot medium [26]. Dynamical friction subsequently brings them to the galaxy center, where they merge with the host system. By redshift $z \simeq 8$, the BHs have settled in the central kiloparsec of a galaxy with stellar mass $\sim 10^9 M_\odot$, establishing a BH-to-stellar-mass ratio of $\sim 1\%$, an order of magnitude above the local relation. After settling, the BHs resume sub-Eddington accretion, maintaining slow but steady growth. For a brief period, the accretion rate reaches the Eddington limit, during which the inferred BH masses and accretion luminosities are consistent with those of observed high-redshift AGN [27]. Our simulation yields a lower limit of a comoving number density of $\sim 10^{-4} \text{ Mpc}^{-3}$ for massive BH-hosting galaxies, consistent with that required to explain the observed LRDs [1, 3, 5, 6].

To demonstrate that such rapid growth is unique to heavy seeds, we also follow the evolution of BHs seeded by Population III remnants ($\sim 800 M_\odot$) formed earlier than the heavy seeds at redshift $z \simeq 22$, hereafter referred to as a light-seed black hole (LBH). Their growth remains highly inefficient. The initial gas supply is strongly suppressed by radiative feedback from the Population III stars, resulting in final masses orders of magnitude smaller than those of the massive seeds (gray line in Fig. 1e). The gas in the host halo quickly photo-evaporates during seed formation because its shallow gravitational potential cannot confine the fuel required for accretion [28]. This contrast highlights the necessity of heavy-seed formation to account for the overmassive BHs already present at $z > 7$.

Fig. 2 shows the time evolution of the most massive BH and the stellar mass of the source galaxy. Points with error bars denote the observed BH and stellar masses of the LRDs, while the blue line traces the simulated relation. Before the formation of the massive seed, the BH mass lies far below the observed values. After the emergence of the heavy seed and its brief phase of super-Eddington growth, the simulated BH mass becomes comparable to the observations, reaching the BH-to-stellar mass ratio above 0.01. Subsequently, the BH and stellar masses co-evolve, while the BH mass remains well above the local scaling relation indicated by the dashed line.

Proto-supermassive stellar system

The progenitor cloud does not form a single collapsing object, but instead undergoes hierarchical fragmentation into a dense multiple system whose members experience sustained supergiant phases that suppress radiative feedback. To examine the feasibility of forming extremely massive seed BHs, we performed a further high-resolution radiation-hydrodynamic simulation for the progenitor cloud of MBH1

that resolves gas densities up to 10^8 cm^{-3} . Figs. 3(a,b) show the gas density distribution during the protostellar evolution. Each protostar accretes mass at a rate of $0.1\text{--}1 M_\odot \text{ yr}^{-1}$, and the most massive one reaches $\sim 4 \times 10^5 M_\odot$ about 2 Myr after the formation of the first protostar (panels c and d). Because of these high accretion rates, the stars remain in an inflated supergiant phase, thereby weakening radiative feedback and allowing continued growth [29]. Fig. 3(e) shows that the stars mostly stay in this supergiant phase, with radii larger than $100 R_\odot$. Due to the bursty nature of accretion, their radii also oscillate with time, repeating cycles of Kelvin–Helmholtz contraction and re-inflation driven by entropy injection. This behavior greatly reduces the UV emissivity and prevents photoevaporation, keeping gas available for subsequent BH growth. The stars collapse into BHs roughly 2 Myr after their formation, marking the end of the high-resolution simulation. At the time of collapse, dense gas remains tightly bound around the stars. These complementary calculations confirm that rapid accretion and limited feedback naturally lead to the formation of supermassive stars that ultimately collapse into heavy BH seeds.

Spectral signatures of circum-BH disks

Dense circum-BH disks in our simulation naturally reproduce the physical conditions required to explain the V-shaped continua and Balmer-series absorption features observed in LRDs [6–8, 30]. Gas at densities $n \gtrsim 10^8 \text{ cm}^{-3}$ enhances the $n = 2$ population of hydrogen, producing strong Balmer absorption [31, 32]. Such high densities imply large electron column densities and hence Thomson optical depths sufficient to broaden the $\text{H}\alpha$ emission line to widths exceeding 1000 km s^{-1} , consistent with observations [8, 33, 34]. Importantly, the $\text{H}\alpha$ emission arises directly from the dense gas around the BHs without requiring an externally imposed broad-line region, closely resembling the recently proposed “BH-star” systems [9, 30, 32, 34, 35].

To compare our heavy-seed BH system with the BH-star interpretation, we carry out a dedicated zoom-in simulation for MBH2, restarting at the moment of seed formation and resolving the circum-BH environment down to 500 au. Fig. 4 shows snapshots at 26 and 523 kyr after BH formation. Shortly after formation, the BH is embedded in a dense, geometrically thick disk with hydrogen densities exceeding $n_H > 10^{10} \text{ cm}^{-3}$, sufficient to maintain a large $n = 2$ population (Fig. 4c). The resulting $\text{H}\alpha$ luminosity within $r < 10^4 \text{ au}$ is $L_{\text{H}\alpha} = 1.5 \times 10^{43} \text{ erg s}^{-1}$, which is comparable to values inferred for LRDs [1, 6]. The Thomson optical depth reaches $\tau_e = 10.2$ at this radius, large enough to generate strong broadening. Although this exceeds observationally inferred values of $\tau_e \sim 0.1\text{--}1$ [8], the effective optical depth for $\text{H}\alpha$ photons is smaller because most of the emission originates near the outer disk ($r \sim 10^4 \text{ au}$). In this early phase, the heavy-seed BH system therefore satisfies the physical conditions associated with the spectral features of a BH-star.

The obscured phase ends after several hundred kyr. At 523 kyr, the BH remains surrounded by dense gas ($n_H \gtrsim 10^8 \text{ cm}^{-3}$) with a moderate Thomson depth of $\tau_e = 0.43$, but the $\text{H}\alpha$ luminosity declines to $5.3 \times 10^{39} \text{ erg s}^{-1}$, below typical LRD values (Fig. 4f). Producing strong $\text{H}\alpha$ emission in this later stage requires additional line emission from the inner ($\lesssim 100 \text{ au}$) region, analogous to a compact broad-line region. The accretion rate remains near the Eddington limit, yielding an inner disk luminosity of $\sim 10^{44} \text{ erg s}^{-1}$, of which 0.1–1% is expected to emerge in $\text{H}\alpha$ [36]. Thomson

scattering in the outer disk then redistributes this radiation and produces broadened emission, yielding $\text{H}\alpha$ luminosities of $10^{41}\text{--}10^{42} \text{ erg s}^{-1}$, consistent with AGNs. These results suggest that the system can naturally transition from an LRD-like, heavily obscured phase into a more AGN-like, less obscured accretion state on timescales of $\sim 0.1\text{--}1 \text{ Myr}$ following the bursty accretion episode.

Implications for early BH populations

Our results demonstrate that heavy-seed formation is a natural outcome of early structure formation in overdense regions, with profound implications for the observed abundance of early quasars and their gravitational-wave signatures. The overmassive BHs produced in these simulations represent plausible progenitors of the first quasars, bridging the gap between the birth of seed BHs and the luminous active nuclei observed by JWST.

Our model shows that BHs can rapidly grow to $\sim 10^7 M_\odot$ through the combination of direct collapse and subsequent super-Eddington accretion. This configuration – a massive BH embedded in a radiation-pressure-supported, optically thick envelope and fed at highly super-Eddington rates – closely resembles the “quasistar” solutions proposed in analytic models [e.g. 35, 37–39]. Our simulations provide a fully cosmological realization of such quasistar-like systems, and follow their formation, migration and subsequent growth within a hierarchically assembling galaxy. This early phase of rapid growth helps overcome the long-standing difficulty that canonical massive BH seeds ($\sim 10^5 M_\odot$) cannot efficiently accrete from hot, feedback-heated gas [26, 40, 41]. While our current simulation does not yet resolve the full galactic gas inflows required to sustain long-term Eddington accretion, it suggests that, once such large-scale supply is captured, the BHs could continue growing to $\sim 10^9 M_\odot$, accounting for the luminous quasars already observed at $z \sim 7$ [42–44].

Although the super-Eddington accretion phase is short compared with the cosmic age, multiple heavy seeds form nearly simultaneously in the vicinity of massive halos, each experiencing a brief period of super-Eddington growth. The presence of several such sources increases the likelihood of observing galaxies in an active, LRD-like phase. Since our calculation covers only a portion of the regions surrounding massive halos, the true occurrence rate of heavy-seed formation may be even higher than inferred here. As these BHs continue to merge during hierarchical galaxy assembly, they are expected to generate strong gravitational-wave signals detectable by the *Laser Interferometer Space Antenna* (LISA). Extrapolating to cosmological scales, the predicted abundance of heavy seeds can account for the luminous quasar population observed by JWST at $z > 7$. Their subsequent coalescences contribute gravitational-wave events with characteristic strains of $h_c \sim 10^{-17}\text{--}10^{-16}$ at millihertz frequencies [45]. Heavy-seed scenarios similar to ours therefore imply LISA event rates of tens to hundreds over a 3-year mission [46, 47]. Taken together, these findings suggest that the early Universe hosted numerous short-lived, rapidly growing BHs that profoundly influenced the assembly of the first massive galaxies.

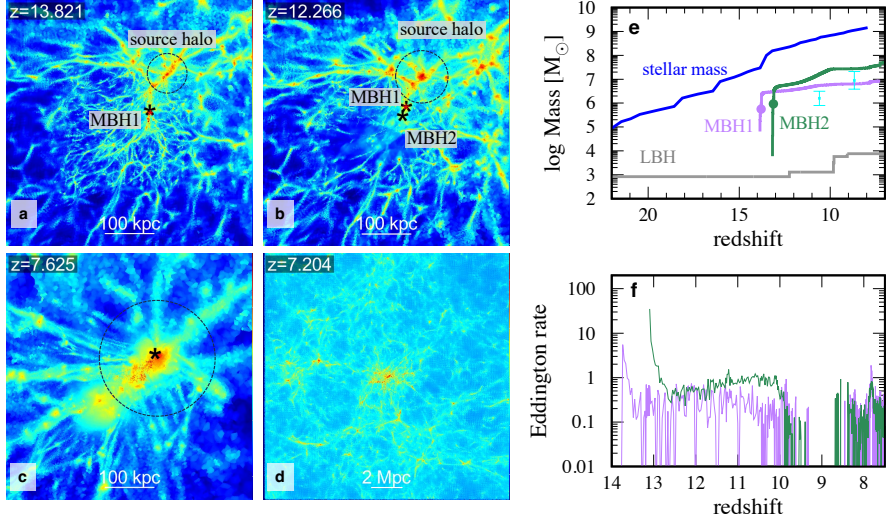


Fig. 1 Formation and evolution of massive seed BHs in the cosmological radiation-hydrodynamic simulation. (a–c) Gas density distributions around the target halos at representative epochs. Black asterisks indicate heavy-seed BHs formed via the collapse of supermassive stars, while red asterisks denote light-seed BHs originating from Population III remnants. The latter almost overlaps with the position of MBH1. Panels (a) and (b) correspond to the epochs when the first (MBH1) and second (MBH2) heavy seeds form, respectively. In panel (c), both MBH1 and MBH2 have migrated into a nearby massive halo and subsequently merged. Dashed circles mark the neighboring source halos that provide the strong FUV radiation required for heavy-seed formation. The radii of the circles indicate their virial radii at each snapshot. (d) Large-scale gas density distribution across the entire simulated volume ($16 h^{-1}$ Mpc on a side), centered on the target halo, shown at the final simulation snapshot. (e) Redshift evolution of the BH masses and the stellar mass of the source galaxy. The gray line shows the growth of a light-seed BH formed at $z \simeq 22$, whereas the purple and green lines correspond to the two heavy seeds (MBH1 and MBH2). Circles mark the moments when the supermassive stars collapse into BHs. The blue line denotes the total stellar mass of the host galaxy. Cyan points with error bars show observed high- z SMBHs [4, 27]. (f) Eddington ratios of the two heavy seeds as a function of redshift. Both MBH1 (purple) and MBH2 (green) undergo short phases of super-Eddington accretion.

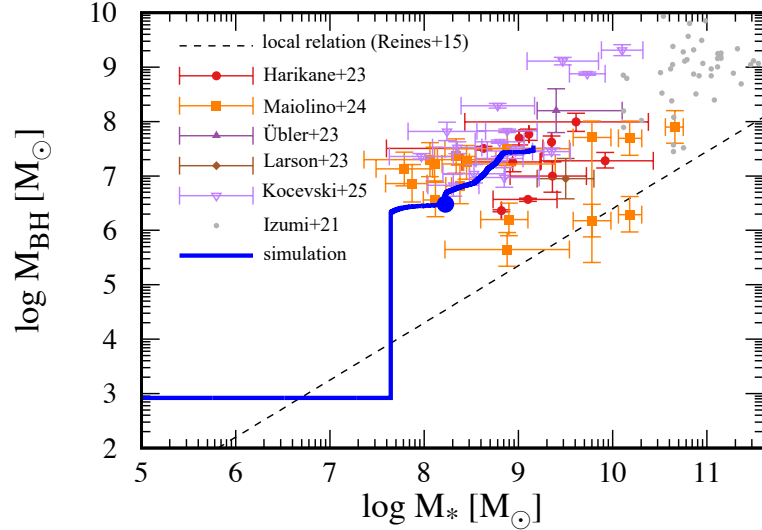


Fig. 2 Time evolution of the most massive BH and the stellar mass of the nearby source galaxy. The solid line shows the simulated evolution of the BH mass (M_{BH}) as a function of the host-galaxy stellar mass (M_*). Observational estimates for LRDs from recent JWST studies [1–3, 27, 48] and for quasars [49] are overplotted for comparison (note that Izumi et al. 49 uses dynamical masses rather than stellar masses). The dashed line indicates the local $M_{\text{BH}}-M_*$ relation derived from nearby galaxies [50]. The blue point marks the time when the BH enters the virial radius of the host halo. Our model naturally reproduces the overmassive BHs observed in LRDs, with M_{BH}/M_* ratios up to an order of magnitude above the local relation.

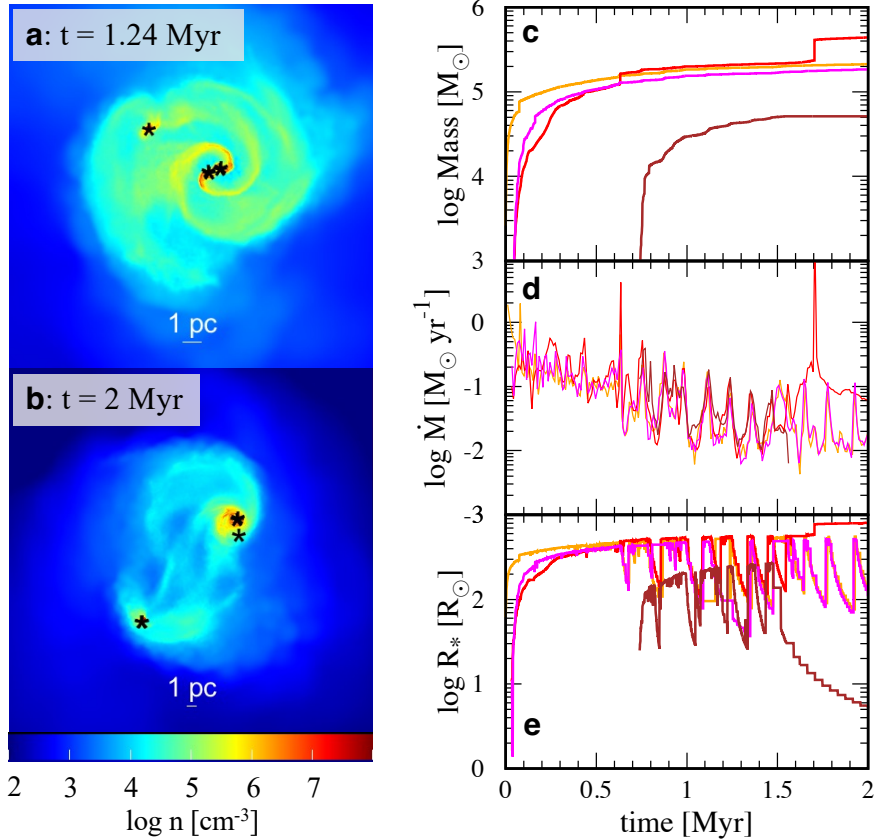


Fig. 3 Formation and evolution of protostars that grow into supermassive stars, which subsequently collapse into MBH1. (a, b) Projected gas density distributions at $t = 1.24$ Myr (panel a) and $t = 2.0$ Myr (panel b), where time is measured from the formation of the first protostar. Asterisks mark protostars with masses exceeding $10^3 M_\odot$. The simulation is terminated at $t = 2$ Myr, corresponding to the typical lifetime of massive stars. Even at the end of the simulation, the stars remain embedded within dense circumstellar and circumbinary disks. (c–e) Time evolution of the stellar mass (panel c), accretion rate (panel d), and stellar radius (panel e) for the four most massive protostars. The stellar masses grow steadily with time, reaching final masses of several $10^5 M_\odot$. Discrete jumps in the mass evolution correspond to stellar mergers, which are accompanied by sharp increases in the accretion rate. The stellar radii expand to 100 – $1000 R_\odot$ as a result of the high mass accretion rates of 0.01 – $1 M_\odot \text{ yr}^{-1}$ [29].

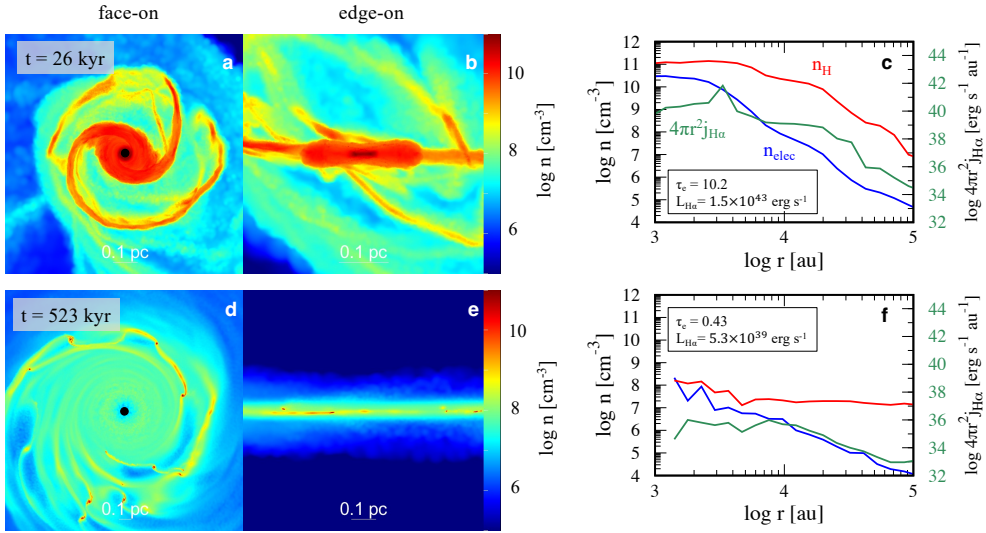


Fig. 4 Formation and evolution of the dense gas disk around MBH2. (a,d) Face-on views of the dense circum-BH disk at $t = 26$ and 523 kyr, showing its rapid emergence and subsequent evolution. (b,e) Edge-on views at the same epochs, illustrating a vertically thick disk at early times that evolves into a thin, rotationally supported structure. (c,f) Radial profiles of the hydrogen number density (red), electron number density (blue), and H α emissivity from gas shells at the corresponding radii (green). Only gas within 30° of the disk plane is included. The estimated H α luminosity and the Thomson-scattering optical depth at $r = 10^4$ au are indicated.

Methods

Our cosmological initial conditions are based on the simulation Phi-4096 of [51]. In this work, a dark-matter-only N -body simulation was performed in a comoving box of side length $16 h^{-1}\text{Mpc}$. The initial condition is generated by MUSIC [52] at a redshift of 127. The adopted cosmological parameters follow the latest measurement by *Planck* [53]: $\Omega_m = 0.31$, $\Omega_\Lambda = 0.69$, $\Omega_b = 0.048$, $h = 0.68$, $n_s = 0.96$, and $\sigma_8 = 0.83$. The simulation employed 4096^3 dark matter particles, corresponding to a particle mass of $5.13 \times 10^3 h^{-1} M_\odot$. This high resolution allows the identification of mini-halos with masses down to $10^5 h^{-1} M_\odot$, sufficient to resolve the sites of Population III (Pop III) star formation and to track chemical enrichment across cosmic time. Halo merger trees were constructed from simulation snapshots between $z = 35$ and $z = 7.5$ using the ROCKSTAR phase space halo/subhalo finder [54] and the CONSISTENT-TREES merger tree code [55]. On top of these, a semi-analytic galaxy formation model was implemented to follow gas cooling, Pop II and Pop III star formation, supernova feedback, metal enrichment, and local Lyman–Werner (LW) radiation fields [17]. We use the result of their model with no baryon streaming motion ($0\sigma_{\text{vbc}}$).

The details of the semi-analytic model largely follow those described in Agarwal et al. [56] with recent updates of the treatment of early star formation [57]. Star formation in Pop II halos follows the standard prescription used in galaxy formation models, in which the cold gas component is converted into stars on a timescale $t_{\text{SF}} = t_{\text{dyn}}/\alpha_*$ with efficiency $\alpha_* = 0.03$ [58]. When the progenitor halos never formed any stars, the stellar population follows a Pop III initial stellar mass function (IMF). The characteristic Pop III stellar mass is determined by the halo mass growth rate, which correlates with the final stellar mass [59]. Stellar populations emit LW radiation that photodissociates molecular hydrogen and delays star formation in nearby halos. The LW radiation intensity is calculated separately for Pop II and Pop III stars [60]:

$$J_{21,\text{III}} = \sum_i 15 \left(\frac{r_i}{1 \text{ kpc}} \right)^{-2} \left(\frac{M_{\text{PopIII},i}}{1000 M_\odot} \right), \quad (1)$$

$$J_{21,\text{II}} = \sum_i 3 \left(\frac{r_i}{1 \text{ kpc}} \right)^{-2} \left(\frac{M_{\text{PopII},i}}{1000 M_\odot} \right), \quad (2)$$

where r_i is the distance to halo i , and $M_{\text{PopIII},i}$ and $M_{\text{PopII},i}$ are the masses of Pop III and Pop II stars formed within the past 5 Myr in halo i , respectively. The sums run over all halos that host Pop III or Pop II star formation. The coefficient in the Pop II expression is derived assuming a Scalo IMF [61] and a stellar metallicity of $Z = 0.001$ [62, 63].

The LW background is primarily contributed by Pop II stars, and its amplitude depends on assumptions regarding the IMF and the stellar models adopted. We note that uncertainties in the LW-intensity modeling have only a minor impact on our results, as we later test explicitly. A halo begins to form Pop III stars once its mass exceeds the critical threshold determined by the local LW intensity [64]. Under strong LW irradiation, star formation is delayed until the halo virial temperature reaches ~ 8000 K, at which point Ly α cooling triggers rapid collapse. Such halos typically

experience high mass accretion rates and host more massive Pop III stars, extending to supermassive stars (SMSs) with $M_* \sim 10^5 M_\odot$, which subsequently collapse into heavy black-hole (BH) seeds. Indeed, Ishiyama and Hirano [17] identified more than $\sim 10^4$ SMSs with the masses larger than $10^5 M_\odot$ as heavy seed candidates in their simulation volume.

From this dataset, we select one representative halo predicted to form a massive seed, which serves as the target of our follow-up radiation-hydrodynamic simulations described in this work. The halo is chosen according to two criteria: (1) the local LW intensity at the time of seed formation exceeds the critical value of $J_{21,\text{crit}} = 1000$, and (2) the halo is not tidally disrupted by nearby massive galaxies. Here, J_{21} denotes the far-ultraviolet (FUV) intensity normalized to $10^{-21} \text{ erg s}^{-1} \text{ Hz}^{-1} \text{ cm}^{-2} \text{ sr}^{-1}$. The second condition is necessary because candidate halos are often located near luminous galaxies that provide strong LW irradiation, but their gravitational collapse may be suppressed by external tidal fields [65]. To exclude such cases, we select halos whose distances from the nearest massive galaxy satisfy $r_{\text{dist}} > 10 d_{\text{tidal}}$, where d_{tidal} is defined as the separation at which the tidal radius imposed by the neighboring galaxy equals the virial radius of the candidate halo. Within the simulated volume, we identify 60 halos that meet both criteria. Among them, we focus on the one that exhibits the most rapid mass growth, reaching a virial temperature of $T_{\text{vir}} \simeq 8 \times 10^3 \text{ K}$, which marks the onset of atomic cooling and subsequent collapse.

We trace back the initial position of the selected candidate halo to the cosmological initial conditions at redshift $z = 127$. A zoom-in region is defined to be 40 times larger than the Lagrangian radius of the target halo, corresponding to a comoving size of $\sim 400 \text{ kpc}$. We confirm that this region is sufficiently large to encompass all material relevant to the formation of the heavy seed BH in the selected halo.

Radiation hydrodynamic calculation

The radiation-hydrodynamic calculation is performed within this zoom-in region using the moving-mesh code AREPO [16], extended to include prescriptions for star formation and BH accretion physics. The resolution of the zoom-in region at the initial snapshot is identical to that used in Ishiyama et al. [51], where the dark-matter particle and baryonic cell masses are 4.33×10^3 and $7.94 \times 10^2 h^{-1} M_\odot$, respectively. At this resolution, star formation within mini-halos can be reliably resolved. Adaptive mesh refinement is applied whenever the local cell size falls below 16 times the local Jeans length, ensuring that gravitational collapse is properly captured and that artificial fragmentation is avoided [66]. Unlike the semi-analytic model of Ishiyama and Hirano [17], the formation and properties of primordial stars are directly followed by the high-resolution radiation-hydrodynamic simulations described here. Uncertainties in the stellar mass and the resulting FUV background intensity in the semi-analytic model may affect whether a heavy-seed BH forms or not, but we later show that these uncertainties do not significantly alter our main conclusion regarding the rapid emergence of overmassive BHs.

We solve a non-equilibrium primordial chemical network consisting of eight species: e^- , H , H^+ , H_2 , H^- , D , D^+ , and HD . The network and associated cooling processes follow the implementation of Matsukoba et al. [67], and include H_2 ro-vibrational line cooling, atomic hydrogen line cooling (including $\text{Ly}\alpha$), and free-free and free-bound

emission of H and H[−]. Heating and chemical reactions induced by FUV, extreme-UV (EUV), and X-ray radiation from nearby stars and BHs are also included, as described later. To avoid numerical contamination from the coarse outer region, gas cells outside the zoom-in volume are kept at fixed resolution, and both radiative cooling and refinement are disabled. In this calculation, we do not explicitly follow the star formation and cooling processes within the nearby massive galaxies that provide the LW background field for the target halo. Instead, we adopt a time-dependent LW intensity derived from the semi-analytic model of Ishiyama and Hirano [17], which self-consistently evolves the star formation and feedback in the same cosmological volume. The resulting LW flux is applied uniformly to all gas cells within the zoom-in region as an isotropic background field. Extended Data Fig. 1 shows the time evolution of the LW intensity contributed by nearby source galaxies. The intensity rises rapidly and exceeds $J_{21} = 1000$ around redshift $z \simeq 18$, the critical level required to suppress H₂ cooling and enable heavy-seed BH formation [e.g., 68–71]. The spectrum of the background radiation is modeled as a blackbody with an effective temperature of $T_{\text{BB}} = 10^5$ K, which reproduces the relative rates of H₂ photodissociation and H[−] photodetachment expected from young star-forming galaxies [69]. We consider the self-shielding of the background LW radiation using the prescription described in Wolcott-Green et al. [72]. We neglect the contribution of ionizing photons from neighboring galaxies, because their mean free path is short and they are strongly attenuated by the surrounding intergalactic medium [73].

During the radiation-hydrodynamic simulation, we do not assume any specific IMF, but instead resolve individual star formation events directly using a sink-particle method. A sink particle is introduced once the local gas density exceeds $2 \times 10^6 \text{ cm}^{-3}$, with an accretion radius set to ten times the local mesh size. The sink accretes surrounding gas following the local gravitational potential, and its properties are updated accordingly at each time step.

Modeling radiation sources

The luminosity and effective temperature of each protostar are determined from its instantaneous mass and accretion rate by interpolating results from one-dimensional stellar evolution models assuming constant accretion rates [74]. If the stellar accretion rate exceeds the critical accretion rate of $\dot{M}_{\text{crit}} \equiv 0.02 M_{\odot} \text{ yr}^{-1}$, we assume the stellar radius expands due to the injection of the large amount of entropy into the stellar envelope [29, 75–77]. During this phase, we assume the surface temperature of the star to be 6000 K and the luminosity to be the Eddington value following the results of detailed stellar evolution calculations [78]. After the accretion rate becomes smaller than \dot{M}_{crit} , we gradually shrink the stellar radius to the radius expected for main-sequence stars on the timescale of the surface Kelvin-Helmholtz (KH) time, which is given by ten times the stellar KH time [79]. Once the stellar age exceeds the lifetime predicted by these models, the star is converted into a BH particle if its final mass exceeds $260 M_{\odot}$ [80]. We note here that all the stars formed during the simulation have a mass above $260 M_{\odot}$ and collapse into the BHs without any supernova feedback. Because the sink radius is much larger than the physical stellar radius, we estimate the final stellar mass from the sink accretion rate using the empirical relation derived

from previous high-resolution simulations of Pop III star formation [59, 81],

$$M_* = 250 M_\odot \left(\frac{\dot{M}_*}{2.8 \times 10^{-3} M_\odot \text{yr}^{-1}} \right)^{0.7}, \quad (3)$$

where \dot{M}_* denotes the time-averaged accretion rate onto the growing protostar. When the stellar age reaches its lifetime, any excess gas mass accreted by the sink that exceeds the estimated stellar mass is returned to the surrounding gas cells to conserve mass. Throughout the simulation, we assign the sink-particle mass as the instantaneous stellar mass when evaluating radiative feedback. This approach somewhat overestimates the stellar luminosity and gives stronger feedback effects compared to the actual stellar mass, so the final stellar mass represents a lower limit to the actual value.

We assume a stellar lifetime of 2 Myr, typical for very massive stars with masses above $100 M_\odot$ [29]. After the stellar age exceeds 2 Myr, we convert the stars into BHs. However, the lifetime of such stars – particularly supermassive stars – remains uncertain. Stars with masses above a few $\times 10^5 M_\odot$ become unstable due to general-relativistic effects and collapse into BHs during the hydrogen-burning phase [29, 82–86]. This implies that collapse may occur earlier than the canonical lifetime assumed for massive stars. Recent calculations [87] show that the threshold mass for general relativistic instability depends on the mass accretion rate, spanning $2\text{--}8 \times 10^5 M_\odot$. If the stars collapse into BHs earlier, the resulting BHs would remain embedded in dense gas for a longer period, thereby extending the phase of super-Eddington growth.

After the stars collapse into BHs, we convert the corresponding sink particles into BH particles. We keep their original accretion radii if the accretion radius is larger than the Bondi radius of the BHs for the ionized gas, otherwise the accretion radii are set to be the Bondi radii. Since the typical accretion radius is around a parsec, the simulations resolve the Bondi radius for most of the massive seed BHs, allowing us to directly follow the gravitational capture of gas onto the BHs. The spectral energy distribution (SED) of accreting BHs is modeled as a double power-law continuum, $F_\nu \propto \nu^{-0.6}$, extending from 1 eV to 10 eV, and $F_\nu \propto \nu^{-1.5}$, extending from 10 eV to 1 keV [88]. This represents the integrated emission from the accretion disk and its associated corona. We allow the accretion rate to exceed the classical Eddington limit, consistent with theoretical models of super-Eddington accretion flows [e.g., 23, 25, 89, 90]. We assume the slim disk solution to give a bolometric luminosity when the accretion rate is higher than the Eddington rate,

$$L_{\text{bol}} = \begin{cases} \epsilon_r \dot{M}_{\text{acc}} c^2 & (\dot{M}_{\text{acc}} \leq 2\dot{M}_{\text{Edd}}), \\ 2 \left[1 + \log \left(\frac{\dot{M}_{\text{acc}}}{\dot{M}_{\text{Edd}}} \right) \right] L_{\text{Edd}} & (\dot{M}_{\text{acc}} > 2\dot{M}_{\text{Edd}}), \end{cases} \quad (4)$$

where $\epsilon_r = 0.1$ is the radiative efficiency, \dot{M}_{acc} is the instantaneous gas accretion rate onto the BH, \dot{M}_{Edd} is the Eddington accretion rate, and $L_{\text{Edd}} \equiv \dot{M}_{\text{Edd}}/\epsilon_r c^2$ is the Eddington luminosity [91]. The emitted radiation is coupled to the surrounding gas through photoionization heating, which regulates the accretion flow and drives

intermittent outflows around the BHs. We do not include any kinetic feedback from the BHs, such as jets or outflows from the unresolved circum-BH disks. We also allow mergers of BHs once the distance between two BHs becomes smaller than 10 physical parsec.

We solve the radiation transfer both from stars and BHs by using RSPH [73, 92], measuring the optical depth from each gas cell to the radiation source based on a ray-tracing method. We consider photo-ionization of H and associated photo-heating, photo-dissociation of H₂ and HD, and photo-detachment of H⁻. The photo-detachment rate of H⁻ is calculated under an optically thin assumption, whereas other photo-reaction rates are calculated using RSPH.

Zoom-in calculation of seed BH formation in the isolated cloud

To assess the feasibility of heavy-seed BH formation, we perform a higher-resolution follow-up simulation that resolves the individual protostars expected to be the progenitors of the seed BHs. We focus on the formation site of the first heavy seed BH, MBH1, identified in the cosmological radiation-hydrodynamic run. This seed, with a final mass of $6 \times 10^5 M_{\odot}$, forms at redshift $z \simeq 14$. We extract a cubic region of 1 comoving kpc on a side centered on the host halo, shortly before the onset of collapse when the central gas density reaches 10^3 cm^{-3} . At this point, the central region of the cloud, of size a few 10 pc, becomes Jeans-unstable (see Extended Data Fig. 4). The re-simulation is performed using the same AREPO framework, but with enhanced spatial and mass resolution to capture the internal fragmentation of the collapsing gas cloud. Sink particles are introduced once the local gas density exceeds $2 \times 10^8 \text{ cm}^{-3}$, representing the formation of individual protostars. The sink radius is set to be four times the cell size, which will be converted into the sink particle, which ranges from 3000–8000 au. We allow mergers of the sink particles once the distance of two sink particles becomes smaller than the sum of the sink radii.

Zoom-in calculation of the BH accretion phase

To reproduce the density structure around the massive seed BH, we performed a high-resolution simulation that resolves gas densities up to 10^{12} cm^{-3} and spatial scales down to 500 au around the central BH. We take the snapshot at the moment when MBH2 forms at $z = 13.1$ and follow the evolution for 30 kyr after its emergence. To capture the later evolution up to 0.5 Myr after MBH2 formation, we also run a complementary simulation with a larger sink radius of 5000 au. Starting from the snapshot at 0.48 Myr, we then reduce the sink radius back to 500 au and continue the calculation to follow the detailed structure of the circum-BH disk for an additional 0.55 kyr. This procedure allows us to track both the long-term disk evolution and the small-scale accretion flow onto the BH.

Estimation of the optical depth and H α luminosity

To estimate the optical depth and H α luminosity, we restrict the analysis to gas cells located within 30° of the disk plane. We estimate the electron column density, N_e , by summing the total number of electrons contained within each spherical shell and dividing by the shell's surface area, yielding an average column density at radius r . The Thomson optical depth is then calculated as $\tau = N_e \sigma_T$, where $\sigma_T = 6.65 \times$

10^{-25} cm^2 is the Thomson scattering cross section. In estimating the $\text{H}\alpha$ luminosity we have assumed case-B recombination. This may underestimate $\text{H}\alpha$ luminosity because resonance scattering will increase the $\text{H}\alpha$ emissivity at densities of $n \sim 10^{10-11} \text{ cm}^{-3}$ [93]. The detailed radiative-transfer calculations for similar conditions indicate that the emergent $\text{H}\alpha/\text{H}\beta$ is enhanced to values of $\sim 6-10$ consistent with the observed values for LRDs [33].

Formation of extremely massive seed BHs

Here we show how extremely massive seed BHs form – through the formation of heavy seeds followed by a brief phase of super-Eddington accretion. Extended Data Fig. 2 shows the time evolution of the mass of the halo that later hosts the heavy seed BH (MBH1). At the time of protostar formation, the halo mass is about $2 \times 10^8 M_\odot$, corresponding to a virial temperature of $4 \times 10^4 \text{ K}$. This is much higher than the canonical virial temperature of 8000 K at which halo collapse is typically expected. Indeed, the semi-analytic model predicts that this halo would have collapsed at $z \sim 18.1$, when its mass was $\sim 10^7 M_\odot$, nearly an order of magnitude smaller than the host halo of MBH1. During the delayed collapse, more gas accumulates within the halo, leading to the formation of more massive stars and enhanced accretion onto the resulting BHs.

Once the gas within a halo becomes gravitationally unstable, it collapses to form stars. The final stellar and BH masses are determined by how much gas is accreted onto the central protostar during its growth phase. Extended Data Fig. 3 shows the radial profiles of (a) gas density, (b) temperature, and (c) escape velocity at the time of protostar formation. The grey line represents the light-seed case (LBH), while the purple and green lines correspond to the two massive seeds, MBH1 and MBH2, respectively. The density structure differs markedly between light and heavy seeds. In the massive-seed cases, the high-density core extends to radii an order of magnitude larger than in the light-seed case, a consequence of the higher gas temperature in the collapsing cloud. Panel (b) shows that the temperature in heavy-seed formation remains near 10^4 K – an order of magnitude higher than in the light-seed case – due to strong UV irradiation that suppresses molecular cooling. The collapse of this larger, hotter core also raises the escape velocity, which exceeds 10 km s^{-1} . This high binding energy facilitates continued mass accretion, as the ionized gas remains gravitationally bound and can feed the central protostar efficiently.

To visualize how gravitational collapse proceeds, we compare the enclosed mass with the critical Bonnor–Ebert (BE) mass, the threshold above which a cloud becomes gravitationally unstable to collapse [94, 95]. The top panels in Extended Data Fig. 4 show the BE mass (green) and the enclosed mass (purple) for LBH, MBH1, and MBH2, from left to right. In the light-seed case, only the innermost 0.1–1 pc region is gravitationally unstable, whereas in the heavy-seed cases the unstable region extends to 10–100 pc. The bottom panels display the ratio of enclosed to BE mass as a function of enclosed mass; regions where this ratio exceeds unity are gravitationally unstable. Only gas within $\sim 10^3 M_\odot$ becomes unstable in the light-seed case, while up to $\sim 10^6 M_\odot$ it is unstable in the heavy-seed cases. These characteristic mass scales roughly correspond to the resulting BH masses: $\sim 800 M_\odot$ for LBH, and 3×10^5 and $6 \times 10^5 M_\odot$ for MBH1 and MBH2, respectively. The dynamical time at the edge of

the gravitationally unstable region is

$$t_{\text{dyn}} \sim \sqrt{\frac{R^3}{GM_{\text{enc}}}} = 1.5 \times 10^7 \text{ yr} \left(\frac{R}{100 \text{ pc}} \right)^{3/2} \left(\frac{M_{\text{enc}}}{10^6 M_{\odot}} \right)^{-1/2}, \quad (5)$$

which is longer than the lifetime of massive stars (~ 2 Myr). This implies that the dense envelope remains bound and should continue to fall onto the BHs after the central protostars collapse, unless feedback from the protostars clears it away.

The temperature decrease at $r \lesssim 1$ pc in MBH2 is caused by the enhanced electron fraction and the subsequent increase in molecular hydrogen formation, similar to the Pop III star formation in a fossil H II region [96]. Extended Data Fig. 5 shows two-dimensional histograms of temperature (left), molecular hydrogen fraction (middle), and electron fraction (right) as functions of gas density, for MBH1 (top) and MBH2 (bottom). Gas at temperature $T \sim 100\text{--}1000$ K in MBH2 shows an enhanced H_2 fraction, indicating that molecular formation and the associated cooling are responsible for the temperature drop. The electron fraction in the outer envelope is almost fully ionized but decreases toward higher densities as recombination proceeds. The elevated electron fraction during collapse promotes H_2 formation through the H^- channel, the dominant pathway in primordial gas, which is catalyzed by free electrons. The ionization source is the strong radiation from MBH1, which fully ionizes and heats the surrounding gas. Indeed, the temperature rise at $r \gtrsim 10^3$ pc in MBH2 indicates that intense radiation from MBH1 photoionizes the intergalactic medium (IGM). Despite the enhanced H_2 formation, a massive seed BH still forms in MBH2, as large-scale gravitational instability drives a strong gas inflow that overwhelms the cooling. This behavior is analogous to the heavy-seed formation in the super-competitive accretion scenario, in which fine-structure lines and dust cooling reduce the gas temperature, while large-scale collapse collects a substantial amount of gas to form massive seed BHs [97, 98].

Robustness tests

To assess numerical robustness and model sensitivity, we performed one higher-resolution run (lv13) and three simulations with reduced FUV background intensities (w2, w5, and w10). In the higher-resolution run, we adopt an effective resolution of 8192^3 in the zoom-in region, corresponding to dark-matter and baryonic particle masses of 542 and $99.2 h^{-1} M_{\odot}$, respectively. This resolution is sufficient to resolve mini-halos in which the first stars form [99, 100]. The run yields results that are nearly identical to the fiducial case: one light-seed BH forms at $z \sim 22$, followed by the formation of two massive seeds. The blue line in Extended Data Fig. 7 shows the evolution of the most massive BH in the higher-resolution run, demonstrating that the mass growth is largely insensitive to the numerical resolution achieved in our default simulation.

To examine uncertainties in the semi-analytic predictions, we also ran simulations with lower FUV background intensities. In our semi-analytic model, the stellar component of the source galaxy is populated using standard galaxy-formation prescriptions, but the star formation rate and efficiency are subject to substantial uncertainty. A

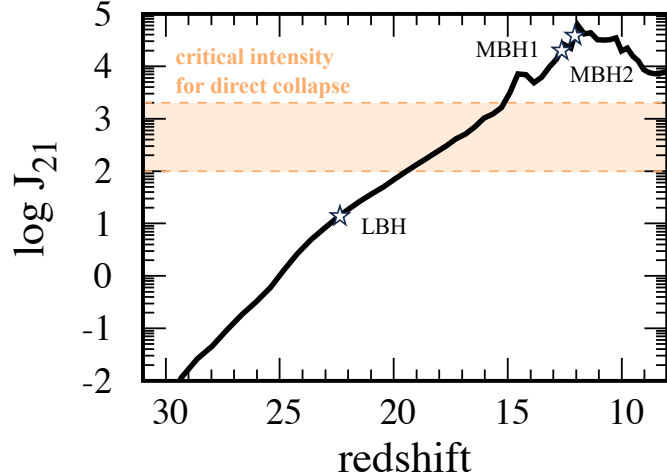
lower star formation efficiency would result in a smaller luminosity and therefore a reduced FUV intensity incident on the massive BH forming halo. The reduced-FUV runs also capture possible spatial variations in the radiation field, which are not explicitly modeled in our semi-analytic treatment. If heavy seeds still form under weaker FUV irradiation, this supports both the robustness of the semi-analytic predictions and the insensitivity to spatial variations.

The green, yellow, and red lines in Extended Data Fig. 7 show the BH mass evolution when the background intensity is reduced by factors of two, five, and ten, respectively. The dependence on the seed formation epoch and subsequent growth is weak. As the FUV intensity decreases, the most massive BH forms slightly earlier, but the difference in formation redshift between the fiducial run and the lowest-intensity case is less than $\Delta z \simeq 0.1$. This behavior is consistent with the expectation that weaker FUV irradiation allows more efficient H_2 cooling, leading to earlier collapse of the target halo. The later mass growth is also only mildly affected: lower FUV intensity results in a somewhat smaller final BH mass, but the variation remains within a factor of three. Even in the weakest-FUV case, the final BH reaches $1.9 \times 10^7 M_\odot$ by $z = 7$, highlighting the robustness of overmassive BH formation despite model uncertainties.

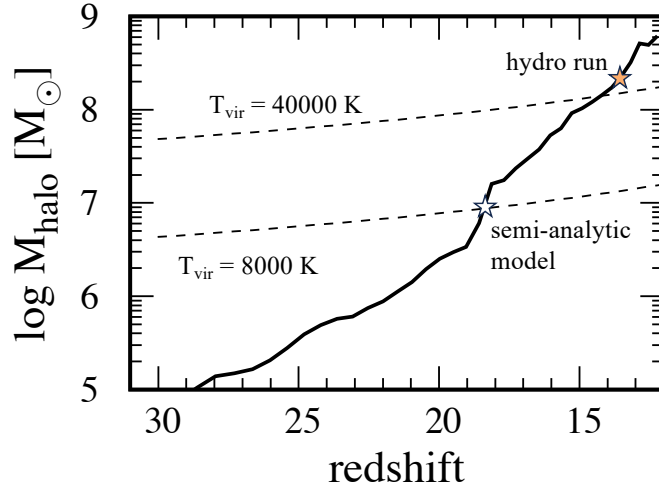
Data Availability. The data underlying this article will be shared on reasonable request to the corresponding author.

Acknowledgements. We thank Kohei Inayoshi for constructive discussions. This work was supported by JSPS KAKENHI Grant Numbers JP21H01122 (T.I), JP21K13960 and JP21H01123 (S.H.). T.I has been supported by IAAR Research Support Program in Chiba University Japan, MEXT as “Program for Promoting Researches on the Supercomputer Fugaku” (JPMXP1020230406), and JICFuS. We conduct numerical simulation on xd-2000 at the Center for Computational Astrophysics (CfCA) of the National Astronomical Observatory of Japan.

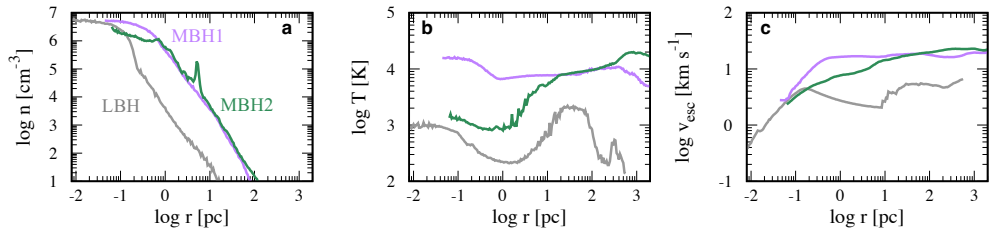
Extended Data



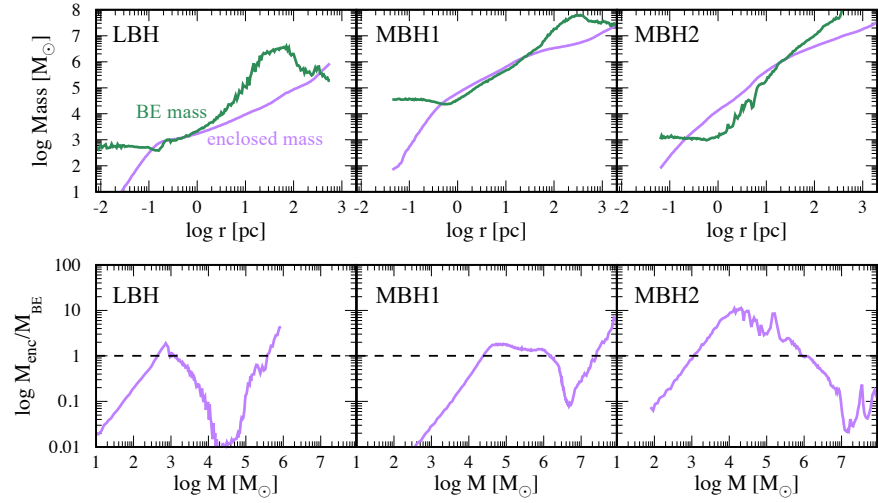
Extended Data Fig. 1 Redshift evolution of the LW radiation intensity (J_{21}) at the location of the target halo. The LW flux gradually increases over time as the stellar mass in the nearby source galaxy grows and the target halo moves closer to the radiation source. The orange shaded region denotes the critical intensity range required for the formation of massive BH seeds ($J_{21,\text{crit}} \simeq 10\text{--}2000$) [68–70]. The redshifts at which the LBH, MBH1, and MBH2 seeds form are also shown.



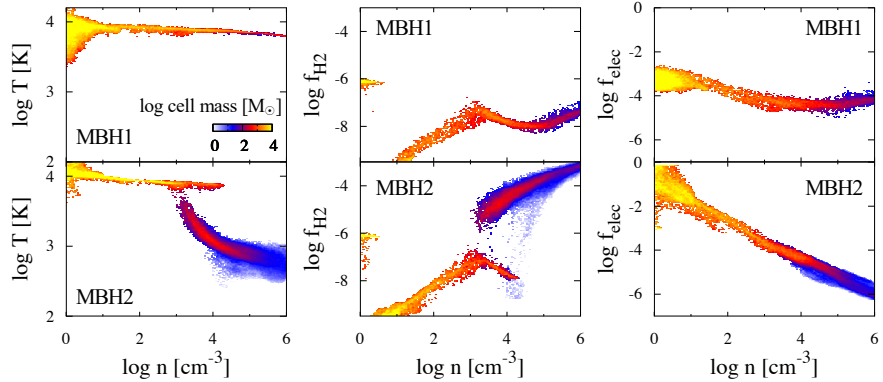
Extended Data Fig. 2 Redshift evolution of the halo mass in which MBH1 forms. The dashed lines indicate halo masses corresponding to virial temperatures of 8000 and 40000 K. The white star symbol marks the redshift at which heavy-seed formation is expected based on the semi-analytic model of Ishiyama and Hirano [17], while the orange star symbol indicates the redshift at which heavy-seed formation occurs in our radiation-hydrodynamic simulation. The delayed onset of cloud collapse allows the halo to accumulate a larger gas reservoir, leading to the formation of an extremely massive seed BH.



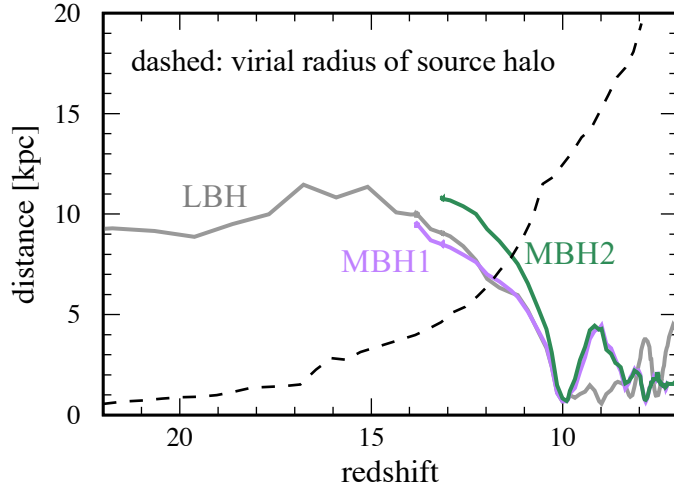
Extended Data Fig. 3 Radial profiles of gas density (a), temperature (b), and escape velocity (c) as functions of distance from the forming protostars. The gray, purple, and green lines correspond to the epochs when the light-seed BH forms at $z \simeq 22$ (LBH) and when the two massive-seed BHs form (MBH1 and MBH2), respectively.



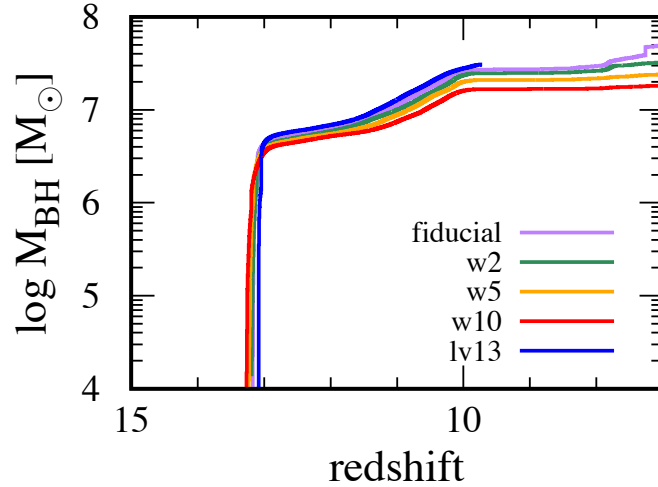
Extended Data Fig. 4 (top) Radial profiles of the Bonnor-Ebert (BE) mass (green) and the enclosed gas mass (purple). Panels from left to right show the profiles for the light-seed (LBH) and massive-seed (MBH1 and MBH2) formation cases. Regions where the enclosed mass exceeds the BE mass are gravitationally unstable and prone to collapse. (bottom) Radial profiles of the ratio between the enclosed mass and the BE mass ($M_{\text{enc}}/M_{\text{BE}}$). The dashed line marks $M_{\text{enc}} = M_{\text{BE}}$, above which the cloud becomes unstable to gravitational collapse. Only the innermost $\sim 10^3 M_{\odot}$ region becomes unstable in the LBH case, whereas up to $\sim 10^6 M_{\odot}$ of gas is unstable in the MBH1 and MBH2 cases.



Extended Data Fig. 5 Two-dimensional histograms of temperature (left), molecular hydrogen fraction (middle), and electron fraction (right) as functions of gas density. The top and bottom panels show the results for MBH1 and MBH2, respectively. Each panel is divided into 200×200 bins, with colors indicating the gas mass in each bin.



Extended Data Fig. 6 Time evolution of the distance between each seed BH and the source halo. The gray, purple, and green lines show the separations of the light-seed BH (LBH), the first massive BH (MBH1), and the second massive BH (MBH2), respectively. The dashed line indicates the evolution of the virial radius of the source halo. The seed BHs are captured by the source halo at redshifts $z \simeq 12$ for LBH and MBH1, and $z \simeq 11.2$ for MBH2.



Extended Data Fig. 7 Time evolution of the most massive BH in the comparison runs. The purple line shows the fiducial run, referred to as MBH2 in the main text. The green, yellow and red lines show the evolution when the luminosity of the source halo in the LW band is reduced by factors of two, five and ten, respectively. The blue line shows the evolution in the higher-resolution run.

References

- [1] Harikane, Y., Zhang, Y., Nakajima, K., Ouchi, M., Isobe, Y., Ono, Y., Hatano, S., Xu, Y., Umeda, H.: A JWST/NIRSpec First Census of Broad-line AGNs at $z = 4\text{--}7$: Detection of 10 Faint AGNs with $M_{BH} 10^6\text{--}10^8 M_{\odot}$ and Their Host Galaxy Properties. *ApJ* **959**(1), 39 (2023) <https://doi.org/10.3847/1538-4357/ad029e> arXiv:2303.11946 [astro-ph.GA]
- [2] Übler, H., Maiolino, R., Curtis-Lake, E., Pérez-González, P.G., Curti, M., Perna, M., Arribas, S., Charlot, S., Marshall, M.A., D'Eugenio, F., Scholtz, J., Bunker, A., Carniani, S., Ferruit, P., Jakobsen, P., Rix, H.-W., Rodríguez Del Pino, B., Willott, C.J., Boeker, T., Cresci, G., Jones, G.C., Kumari, N., Rawle, T.: GA-NIFS: A massive black hole in a low-metallicity AGN at $z \sim 5.55$ revealed by JWST/NIRSpec IFS. *A&A* **677**, 145 (2023) <https://doi.org/10.1051/0004-6361/202346137> arXiv:2302.06647 [astro-ph.GA]
- [3] Maiolino, R., Scholtz, J., Curtis-Lake, E., Carniani, S., Baker, W., de Graaff, A., Tacchella, S., Übler, H., D'Eugenio, F., Witstok, J., Curti, M., Arribas, S., Bunker, A.J., Charlot, S., Chevallard, J., Eisenstein, D.J., Egami, E., Ji, Z., Jones, G.C., Lyu, J., Rawle, T., Robertson, B., Rujopakarn, W., Perna, M., Sun, F., Venturi, G., Williams, C.C., Willott, C.: JADES: The diverse population of infant black holes at $4 < z < 11$: Merging, tiny, poor, but mighty. *A&A* **691**, 145 (2024) <https://doi.org/10.1051/0004-6361/202347640> arXiv:2308.01230 [astro-ph.GA]
- [4] Maiolino, R., Scholtz, J., Witstok, J., Carniani, S., D'Eugenio, F., de Graaff, A., Übler, H., Tacchella, S., Curtis-Lake, E., Arribas, S., Bunker, A., Charlot, S., Chevallard, J., Curti, M., Looser, T.J., Maseda, M.V., Rawle, T.D., Rodríguez del Pino, B., Willott, C.J., Egami, E., Eisenstein, D.J., Hainline, K.N., Robertson, B., Williams, C.C., Willmer, C.N.A., Baker, W.M., Boyett, K., DeCoursey, C., Fabian, A.C., Helton, J.M., Ji, Z., Jones, G.C., Kumari, N., Laporte, N., Nelson, E.J., Perna, M., Sandles, L., Shvaei, I., Sun, F.: A small and vigorous black hole in the early Universe. *Nature* **627**(8002), 59–63 (2024) <https://doi.org/10.1038/s41586-024-07052-5> arXiv:2305.12492 [astro-ph.GA]
- [5] Taylor, A.J., Finkelstein, S.L., Kocevski, D.D., Jeon, J., Bromm, V., Amorín, R.O., Arrabal Haro, P., Backhaus, B.E., Bagley, M.B., Banados, E., Bhatawdekar, R., Brooks, M., Calabró, A., Chávez Ortiz, Ó.A., Cheng, Y., Cleri, N.J., Cole, J.W., Davis, K., Dickinson, M., Donnan, C., Dunlop, J.S., Ellis, R.S., Fernández, V., Fontana, A., Fujimoto, S., Giavalisco, M., Grazian, A., Guo, J., Hathi, N.P., Holwerda, B.W., Hirschmann, M., Inayoshi, K., Kartaltepe, J.S., Khusanova, Y., Koekemoer, A.M., Kokorev, V., Larson, R.L., Leung, G.C.K., Lucas, R.A., McLeod, D.J., Napolitano, L., Onoue, M., Pacucci, F., Papovich, C., Pérez-González, P.G., Pirzkal, N., Somerville, R.S., Trump, J.R., Wilkins, S.M., Yung, L.Y.A., Zhang, H.: Broad-line AGNs at $3.5 < z < 6$: The Black Hole Mass Function and a Connection with Little Red Dots. *ApJ* **986**(2), 165 (2025)

<https://doi.org/10.3847/1538-4357/add15b> arXiv:2409.06772 [astro-ph.GA]

- [6] Matthee, J., Naidu, R.P., Brammer, G., Chisholm, J., Eilers, A.-C., Goulding, A., Greene, J., Kashino, D., Labbe, I., Lilly, S.J., Mackenzie, R., Oesch, P.A., Weibel, A., Wuyts, S., Xiao, M., Bordoloi, R., Bouwens, R., van Dokkum, P., Illingworth, G., Kramarenko, I., Maseda, M.V., Mason, C., Meyer, R.A., Nelson, E.J., Reddy, N.A., Shvarei, I., Simcoe, R.A., Yue, M.: Little Red Dots: An Abundant Population of Faint Active Galactic Nuclei at $z \sim 5$ Revealed by the EIGER and FRESCO JWST Surveys. *ApJ* **963**(2), 129 (2024) <https://doi.org/10.3847/1538-4357/ad2345> arXiv:2306.05448 [astro-ph.GA]
- [7] Hvizing, R.E., de Graaff, A., Miller, T.B., Setton, D.J., Greene, J.E., Labb  , I., Brammer, G., Bezanson, R., Boogaard, L.A., Cleri, N.J., Leja, J., Maseda, M.V., McConachie, I., Matthee, J., Naidu, R.P., Oesch, P.A., Wang, B., Whitaker, K.E., Williams, C.C.: RUBIES: A spectroscopic census of little red dots: All point sources with v-shaped continua have broad lines. *A&A* **702**, 57 (2025) <https://doi.org/10.1051/0004-6361/202555816> arXiv:2506.05459 [astro-ph.GA]
- [8] Rusakov, V., Watson, D., Nikopoulos, G.P., Brammer, G., Gottumukkala, R., Harvey, T., Heintz, K.E., Nielsen, R.D., Sim, S.A., Sneppen, A., Vijayan, A.P., Adams, N., Austin, D., Conselice, C.J., Goolsby, C.M., Toft, S., Wittstok, J.: JWST's little red dots: an emerging population of young, low-mass AGN cocooned in dense ionized gas. *arXiv e-prints*, 2503-16595 (2025) <https://doi.org/10.48550/arXiv.2503.16595> arXiv:2503.16595 [astro-ph.GA]
- [9] Naidu, R.P., Matthee, J., Katz, H., de Graaff, A., Oesch, P., Smith, A., Greene, J.E., Brammer, G., Weibel, A., Hvizing, R., Chisholm, J., Labb  , I., Simcoe, R.A., Witten, C., Atek, H., Baggen, J.F.W., Belli, S., Bezanson, R., Boogaard, L.A., Bose, S., Covelo-Paz, A., Dayal, P., Fudamoto, Y., Furtak, L.J., Giovinazzo, E., Goulding, A., Gronke, M., Heintz, K.E., Hirschmann, M., Illingworth, G., Inoue, A.K., Johnson, B.D., Leja, J., Leonova, E., McConachie, I., Maseda, M.V., Natarajan, P., Nelson, E., Setton, D.J., Shvarei, I., Sobral, D., Stefanon, M., Tacchella, S., Toft, S., Torralba, A., van Dokkum, P., van der Wel, A., Volonteri, M., Walter, F., Wang, B., Watson, D.: A "Black Hole Star" Reveals the Remarkable Gas-Enshrouded Hearts of the Little Red Dots. *arXiv e-prints*, 2503-16596 (2025) <https://doi.org/10.48550/arXiv.2503.16596> arXiv:2503.16596 [astro-ph.GA]
- [10] de Graaff, A., Brammer, G., Weibel, A., Lewis, Z., Maseda, M.V., Oesch, P.A., Bezanson, R., Boogaard, L.A., Cleri, N.J., Cooper, O.R., Gottumukkala, R., Greene, J.E., Hirschmann, M., Hvizing, R.E., Katz, H., Labb  , I., Leja, J., Matthee, J., McConachie, I., Miller, T.B., Naidu, R.P., Price, S.H., Rix, H.-W., Setton, D.J., Suess, K.A., Wang, B., Whitaker, K.E., Williams, C.C.: RUBIES: A complete census of the bright and red distant Universe with JWST/NIRSpec. *A&A* **697**, 189 (2025) <https://doi.org/10.1051/0004-6361/202452186> arXiv:2409.05948 [astro-ph.GA]

- [11] Lupi, A., Quadri, G., Volonteri, M., Colpi, M., Regan, J.A.: Sustained super-Eddington accretion in high-redshift quasars. *A&A* **686**, 256 (2024) <https://doi.org/10.1051/0004-6361/202348788> arXiv:2312.08422 [astro-ph.GA]
- [12] Trinca, A., Valiante, R., Schneider, R., Juodžbalis, I., Maiolino, R., Graziani, L., Lupi, A., Natarajan, P., Volonteri, M., Zana, T.: Episodic super-Eddington accretion as a clue to Overmassive Black Holes in the early Universe. arXiv e-prints, 2412–14248 (2024) <https://doi.org/10.48550/arXiv.2412.14248> arXiv:2412.14248 [astro-ph.GA]
- [13] Jeon, J., Liu, B., Bromm, V., Fujimoto, S., Taylor, A.J., Kokorev, V., Larson, R.L., Chisholm, J., Finkelstein, S.L., Kocevski, D.D.: Little Red Dots and their Progenitors from Direct Collapse Black Holes. arXiv e-prints, 2508–14155 (2025) <https://doi.org/10.48550/arXiv.2508.14155> arXiv:2508.14155 [astro-ph.GA]
- [14] Matthee, J., Naidu, R.P., Kotiwale, G., Furtak, L.J., Kramarenko, I., Mackenzie, R., Greene, J., Adamo, A., Bouwens, R.J., Di Cesare, C., Eilers, A.-C., de Graaff, A., Heintz, K.E., Kashino, D., Maseda, M.V., Tacchella, S., Torralba, A.: Environmental Evidence for Overly Massive Black Holes in Low-mass Galaxies and a Black Hole–Halo Mass Relation at $z \sim 5$. *ApJ* **988**(2), 246 (2025) <https://doi.org/10.3847/1538-4357/ade886> arXiv:2412.02846 [astro-ph.GA]
- [15] Bulichi, T.-E., Zier, O., Smith, A., Vogelsberger, M., Eilers, A.-C., Kannan, R., Shen, X., Puchwein, E., Garaldi, E., Borrow, J.: High-redshift AGN population in radiation-hydrodynamics simulations. *MNRAS* **544**(1), 355–371 (2025) <https://doi.org/10.1093/mnras/staf1769> arXiv:2507.11605 [astro-ph.GA]
- [16] Springel, V.: E pur si muove: Galilean-invariant cosmological hydrodynamical simulations on a moving mesh. *MNRAS* **401**(2), 791–851 (2010) <https://doi.org/10.1111/j.1365-2966.2009.15715.x> arXiv:0901.4107 [astro-ph.CO]
- [17] Ishiyama, T., Hirano, S.: A Semi-analytic Framework of Population III and Subsequent Galaxy Formation on Cosmological N-body Simulations. arXiv e-prints, 2501–17540 (2025) <https://doi.org/10.48550/arXiv.2501.17540> arXiv:2501.17540 [astro-ph.GA]
- [18] Chon, S., Hosokawa, T., Yoshida, N.: Radiation hydrodynamics simulations of the formation of direct-collapse supermassive stellar systems. *MNRAS* **475**, 4104–4121 (2018) <https://doi.org/10.1093/mnras/sty086> arXiv:1711.05262
- [19] Wise, J.H., Regan, J.A., O’Shea, B.W., Norman, M.L., Downes, T.P., Xu, H.: Formation of massive black holes in rapidly growing pre-galactic gas clouds. *Nature* **566**(7742), 85–88 (2019) <https://doi.org/10.1038/s41586-019-0873-4> arXiv:1901.07563 [astro-ph.GA]
- [20] Regan, J.A., Wise, J.H., Woods, T.E., Downes, T.P., O’Shea, B.W., Norman, M.L.: The Formation of Very Massive Stars in Early Galaxies and Implications

for Intermediate Mass Black Holes. *The Open Journal of Astrophysics* **3**(1), 15 (2020) <https://doi.org/10.21105/astro.2008.08090> arXiv:2008.08090 [astro-ph.GA]

[21] Latif, M.A., Whalen, D.J., Khochfar, S., Herrington, N.P., Woods, T.E.: Turbulent cold flows gave birth to the first quasars. *Nature* **607**(7917), 48–51 (2022) <https://doi.org/10.1038/s41586-022-04813-y> arXiv:2207.05093 [astro-ph.GA]

[22] Kiyuna, M., Hosokawa, T., Chon, S.: Sequential formation of supermassive stars and heavy seed BHs through the interplay of cosmological cold accretion and stellar radiative feedback. *MNRAS* **534**(4), 3916–3935 (2024) <https://doi.org/10.1093/mnras/stae2380> arXiv:2408.14534 [astro-ph.GA]

[23] Begelman, M.C.: Black holes in radiation-dominated gas: an analogue of the Bondi accretion problem. *MNRAS* **184**, 53–67 (1978) <https://doi.org/10.1093/mnras/184.1.53>

[24] Ohsuga, K., Mori, M., Nakamoto, T., Mineshige, S.: Supercritical Accretion Flows around Black Holes: Two-dimensional, Radiation Pressure-dominated Disks with Photon Trapping. *ApJ* **628**(1), 368–381 (2005) <https://doi.org/10.1086/430728> arXiv:astro-ph/0504168 [astro-ph]

[25] Sadowski, A., Narayan, R.: Three-dimensional simulations of supercritical black hole accretion discs - luminosities, photon trapping and variability. *MNRAS* **456**(4), 3929–3947 (2016) <https://doi.org/10.1093/mnras/stv2941> arXiv:1509.03168 [astro-ph.HE]

[26] Chon, S., Hosokawa, T., Omukai, K.: Cosmological direct-collapse black hole formation sites hostile for their growth. *MNRAS* **502**(1), 700–713 (2021) <https://doi.org/10.1093/mnras/stab061> arXiv:2008.09120 [astro-ph.GA]

[27] Larson, R.L., Finkelstein, S.L., Kocevski, D.D., Hutchison, T.A., Trump, J.R., Arrabal Haro, P., Bromm, V., Cleri, N.J., Dickinson, M., Fujimoto, S., Kartaltepe, J.S., Koekemoer, A.M., Papovich, C., Pirzkal, N., Tacchella, S., Zavala, J.A., Bagley, M., Behroozi, P., Champagne, J.B., Cole, J.W., Jung, I., Morales, A.M., Yang, G., Zhang, H., Zitrin, A., Amorín, R.O., Burgarella, D., Casey, C.M., Chávez Ortiz, Ó.A., Cox, I.G., Chwiorowsky, K., Fontana, A., Gawiser, E., Grazian, A., Grogin, N.A., Harish, S., Hathi, N.P., Hirschmann, M., Holwerda, B.W., Juneau, S., Leung, G.C.K., Lucas, R.A., McGrath, E.J., Pérez-González, P.G., Rigby, J.R., Seillé, L.-M., Simons, R.C., de La Vega, A., Weiner, B.J., Wilkins, S.M., Yung, L.Y.A., Ceers Team: A CEERS Discovery of an Accreting Supermassive Black Hole 570 Myr after the Big Bang: Identifying a Progenitor of Massive $z > 6$ Quasars. *ApJ* **953**(2), 29 (2023) <https://doi.org/10.3847/2041-8213/ace619> arXiv:2303.08918 [astro-ph.GA]

[28] Alvarez, M.A., Wise, J.H., Abel, T.: Accretion onto the First Stellar-Mass Black Holes. *ApJ* **701**(2), 133–137 (2009) <https://doi.org/10.1088/0004-637X/701/2/>

L133 arXiv:0811.0820 [astro-ph]

- [29] Hosokawa, T., Yorke, H.W., Inayoshi, K., Omukai, K., Yoshida, N.: Formation of Primordial Supermassive Stars by Rapid Mass Accretion. *ApJ* **778**(2), 178 (2013) <https://doi.org/10.1088/0004-637X/778/2/178> arXiv:1308.4457 [astro-ph.SR]
- [30] de Graaff, A., Rix, H.-W., Naidu, R.P., Labb  , I., Wang, B., Leja, J., Matthee, J., Katz, H., Greene, J.E., Hviding, R.E., Baggen, J., Bezanson, R., Boogaard, L.A., Brammer, G., Dayal, P., van Dokkum, P., Goulding, A.D., Hirschmann, M., Maseda, M.V., McConachie, I., Miller, T.B., Nelson, E., Oesch, P.A., Setton, D.J., Shvarei, I., Weibel, A., Whitaker, K.E., Williams, C.C.: A remarkable ruby: Absorption in dense gas, rather than evolved stars, drives the extreme Balmer break of a little red dot at $z = 3.5$. *A&A* **701**, 168 (2025) <https://doi.org/10.1051/0004-6361/202554681> arXiv:2503.16600 [astro-ph.GA]
- [31] Ferland, G.J., Chatzikos, M., Guzm  , F., Lykins, M.L., van Hoof, P.A.M., Williams, R.J.R., Abel, N.P., Badnell, N.R., Keenan, F.P., Porter, R.L., Stan-cil, P.C.: The 2017 Release Cloudy. *Rev. Mexicana Astron. Astrofis.* **53**, 385–438 (2017) <https://doi.org/10.48550/arXiv.1705.10877> arXiv:1705.10877 [astro-ph.GA]
- [32] Inayoshi, K., Maiolino, R.: Extremely Dense Gas around Little Red Dots and High-redshift Active Galactic Nuclei: A Nonstellar Origin of the Balmer Break and Absorption Features. *ApJ* **980**(2), 27 (2025) <https://doi.org/10.3847/2041-8213/adaebd> arXiv:2409.07805 [astro-ph.GA]
- [33] Chang, S.-J., Gronke, M., Matthee, J., Mason, C.: Impact of Resonance, Raman, and Thomson Scattering on Hydrogen Line Formation in Little Red Dots. *arXiv e-prints*, 2508–08768 (2025) <https://doi.org/10.48550/arXiv.2508.08768> arXiv:2508.08768 [astro-ph.GA]
- [34] Torralba, A., Matthee, J., Pezzulli, G., Naidu, R.P., Ishikawa, Y., Brammer, G.B., Chang, S.-J., Chisholm, J., de Graaff, A., D'Eugenio, F., Di Cesare, C., Eilers, A.-C., Greene, J.E., Gronke, M., Iani, E., Kokorev, V., Kotiwale, G., Kramarenko, I., Ma, Y., Mascia, S., Navarrete, B., Nelson, E., Oesch, P., Simcoe, R.A., Wuyts, S.: The warm outer layer of a Little Red Dot as the source of [Fe II] and collisional Balmer lines with scattering wings. *arXiv e-prints*, 2510–00103 (2025) <https://doi.org/10.48550/arXiv.2510.00103> arXiv:2510.00103 [astro-ph.GA]
- [35] Kido, D., Ioka, K., Hotokezaka, K., Inayoshi, K., Irwin, C.M.: Black Hole Envelopes in Little Red Dots. *MNRAS* (2025) <https://doi.org/10.1093/mnras/staf1898> arXiv:2505.06965 [astro-ph.HE]
- [36] Greene, J.E., Ho, L.C.: Estimating Black Hole Masses in Active Galaxies Using the $H\alpha$ Emission Line. *ApJ* **630**(1), 122–129 (2005) <https://doi.org/10.1086/>

431897 arXiv:astro-ph/0508335 [astro-ph]

- [37] Begelman, M.C., Rossi, E.M., Armitage, P.J.: Quasi-stars: accreting black holes inside massive envelopes. *MNRAS* **387**(4), 1649–1659 (2008) <https://doi.org/10.1111/j.1365-2966.2008.13344.x> arXiv:0711.4078 [astro-ph]
- [38] Volonteri, M.: Formation of supermassive black holes. *A&A Rev.* **18**(3), 279–315 (2010) <https://doi.org/10.1007/s00159-010-0029-x> arXiv:1003.4404 [astro-ph.CO]
- [39] Santarelli, A.D., Farag, E., Bellinger, E.P., Natarajan, P., Naidu, R.P., Campbell, C.B., Caplan, M.E.: Evolutionary Tracks and Spectral Properties of Quasi-stars and Their Correlation with Little Red Dots. *arXiv e-prints*, 2510–17952 (2025) <https://doi.org/10.48550/arXiv.2510.17952> arXiv:2510.17952 [astro-ph.GA]
- [40] Dubois, Y., Devriendt, J., Slyz, A., Teyssier, R.: Self-regulated growth of supermassive black holes by a dual jet-heating active galactic nucleus feedback mechanism: methods, tests and implications for cosmological simulations. *MNRAS* **420**(3), 2662–2683 (2012) <https://doi.org/10.1111/j.1365-2966.2011.20236.x> arXiv:1108.0110 [astro-ph.CO]
- [41] Latif, M.A., Volonteri, M., Wise, J.H.: Early growth of typical high-redshift black holes seeded by direct collapse. *MNRAS* **476**(4), 5016–5025 (2018) <https://doi.org/10.1093/mnras/sty622> arXiv:1801.07685 [astro-ph.GA]
- [42] Mortlock, D.J., Warren, S.J., Venemans, B.P., Patel, M., Hewett, P.C., McMahon, R.G., Simpson, C., Theuns, T., González-Solares, E.A., Adamson, A., Dye, S., Hambly, N.C., Hirst, P., Irwin, M.J., Kuiper, E., Lawrence, A., Röttgering, H.J.A.: A luminous quasar at a redshift of $z = 7.085$. *Nature* **474**(7353), 616–619 (2011) <https://doi.org/10.1038/nature10159> arXiv:1106.6088 [astro-ph.CO]
- [43] Bañados, E., Venemans, B.P., Mazzucchelli, C., Farina, E.P., Walter, F., Wang, F., Decarli, R., Stern, D., Fan, X., Davies, F.B., Hennawi, J.F., Simcoe, R.A., Turner, M.L., Rix, H.-W., Yang, J., Kelson, D.D., Rudie, G.C., Winters, J.M.: An 800-million-solar-mass black hole in a significantly neutral Universe at a redshift of 7.5. *Nature* **553**(7689), 473–476 (2018) <https://doi.org/10.1038/nature25180> arXiv:1712.01860 [astro-ph.GA]
- [44] Wang, F., Yang, J., Fan, X., Hennawi, J.F., Barth, A.J., Banados, E., Bian, F., Boutsia, K., Connor, T., Davies, F.B., Decarli, R., Eilers, A.-C., Farina, E.P., Green, R., Jiang, L., Li, J.-T., Mazzucchelli, C., Nanni, R., Schindler, J.-T., Venemans, B., Walter, F., Wu, X.-B., Yue, M.: A Luminous Quasar at Redshift 7.642. *ApJ* **907**(1), 1 (2021) <https://doi.org/10.3847/2041-8213/abd8c6> arXiv:2101.03179 [astro-ph.GA]
- [45] DeGraf, C., Chen, N., Ni, Y., Di Matteo, T., Bird, S., Tremmel, M., Croft,

R.: High-redshift supermassive black hole mergers in simulations with dynamical friction modelling. *MNRAS* **527**(4), 11766–11776 (2024) <https://doi.org/10.1093/mnras/stad3084> arXiv:2302.00702 [astro-ph.GA]

[46] Sesana, A., Volonteri, M., Haardt, F.: The imprint of massive black hole formation models on the LISA data stream. *MNRAS* **377**(4), 1711–1716 (2007) <https://doi.org/10.1111/j.1365-2966.2007.11734.x> arXiv:astro-ph/0701556 [astro-ph]

[47] McCaffrey, J., Regan, J., Smith, B., Wise, J., O’Shea, B., Norman, M.: A Heavy Seed Black Hole Mass Function at High Redshift – Prospects for LISA. *The Open Journal of Astrophysics* **8**, 11 (2025) <https://doi.org/10.33232/001c.129138> arXiv:2409.16413 [astro-ph.GA]

[48] Kocevski, D.D., Finkelstein, S.L., Barro, G., Taylor, A.J., Calabro, A., Laloux, B., Buchner, J., Trump, J.R., Leung, G.C.K., Yang, G., Dickinson, M., Pérez-González, P.G., Pacucci, F., Inayoshi, K., Somerville, R.S., McGrath, E.J., Akins, H.B., Bagley, M.B., Bowler, R.A.A., Bisigello, L., Carnall, A., Casey, C.M., Cheng, Y., Cleri, N.J., Costantin, L., Cullen, F., Davis, K., Donnan, C.T., Dunlop, J.S., Ellis, R.S., Ferguson, H.C., Fujimoto, S., Fontana, A., Giavalisco, M., Grazian, A., Grogin, N.A., Hathi, N.P., Hirschmann, M., Huertas-Company, M., Holwerda, B.W., Illingworth, G., Juneau, S., Kartaltepe, J.S., Koekemoer, A.M., Li, W., Lucas, R.A., Magee, D., Mason, C., McLeod, D.J., McLure, R.J., Napolitano, L., Papovich, C., Pirzkal, N., Rodighiero, G., Santini, P., Wilkins, S.M., Yung, L.Y.A.: The Rise of Faint, Red Active Galactic Nuclei at $z > 4$: A Sample of Little Red Dots in the JWST Extragalactic Legacy Fields. *ApJ* **986**(2), 126 (2025) <https://doi.org/10.3847/1538-4357/adbc7d> arXiv:2404.03576 [astro-ph.GA]

[49] Izumi, T., Matsuoka, Y., Fujimoto, S., Onoue, M., Strauss, M.A., Umehata, H., Imanishi, M., Kohno, K., Kawaguchi, T., Kawamuro, T., Baba, S., Nagao, T., Toba, Y., Inayoshi, K., Silverman, J.D., Inoue, A.K., Ikarashi, S., Iwasawa, K., Kashikawa, N., Hashimoto, T., Nakanishi, K., Ueda, Y., Schramm, M., Lee, C.-H., Suh, H.: Subaru High- z Exploration of Low-luminosity Quasars (SHELLQs). XIII. Large-scale Feedback and Star Formation in a Low-luminosity Quasar at $z = 7.07$ on the Local Black Hole to Host Mass Relation. *ApJ* **914**(1), 36 (2021) <https://doi.org/10.3847/1538-4357/abf6dc> arXiv:2104.05738 [astro-ph.GA]

[50] Reines, A.E., Volonteri, M.: Relations between Central Black Hole Mass and Total Galaxy Stellar Mass in the Local Universe. *ApJ* **813**(2), 82 (2015) <https://doi.org/10.1088/0004-637X/813/2/82> arXiv:1508.06274 [astro-ph.GA]

[51] Ishiyama, T., Prada, F., Klypin, A.A., Sinha, M., Metcalf, R.B., Jullo, E., Altieri, B., Cora, S.A., Croton, D., de la Torre, S., Millán-Calero, D.E., Oogi, T., Ruedas, J., Vega-Martínez, C.A.: The Uchuu simulations: Data Release 1 and dark matter halo concentrations. *MNRAS* **506**(3), 4210–4231 (2021) <https://doi.org/10.1093/mnras/stab1755> arXiv:2007.14720 [astro-ph.CO]

[52] Hahn, O., Abel, T.: Multi-scale initial conditions for cosmological simulations. *MNRAS* **415**(3), 2101–2121 (2011) <https://doi.org/10.1111/j.1365-2966.2011.18820.x> [arXiv:1103.6031](https://arxiv.org/abs/1103.6031) [astro-ph.CO]

[53] Planck Collaboration, Aghanim, N., Akrami, Y., Ashdown, M., Aumont, J., Baccigalupi, C., Ballardini, M., Banday, A.J., Barreiro, R.B., Bartolo, N., Basak, S., Battye, R., Benabed, K., Bernard, J.-P., Bersanelli, M., Bielewicz, P., Bock, J.J., Bond, J.R., Borrill, J., Bouchet, F.R., Boulanger, F., Bucher, M., Burigana, C., Butler, R.C., Calabrese, E., Cardoso, J.-F., Carron, J., Challinor, A., Chiang, H.C., Chluba, J., Colombo, L.P.L., Combet, C., Contreras, D., Crill, B.P., Cuttaia, F., de Bernardis, P., de Zotti, G., Delabrouille, J., Delouis, J.-M., Di Valentino, E., Diego, J.M., Doré, O., Douspis, M., Ducout, A., Dupac, X., Dusini, S., Efstathiou, G., Elsner, F., Enßlin, T.A., Eriksen, H.K., Fantaye, Y., Farhang, M., Fergusson, J., Fernandez-Cobos, R., Finelli, F., Forastieri, F., Frailis, M., Fraisse, A.A., Franceschi, E., Frolov, A., Galeotta, S., Galli, S., Ganga, K., Génova-Santos, R.T., Gerbino, M., Ghosh, T., González-Nuevo, J., Górski, K.M., Gratton, S., Gruppuso, A., Gudmundsson, J.E., Hamann, J., Handley, W., Hansen, F.K., Herranz, D., Hildebrandt, S.R., Hivon, E., Huang, Z., Jaffe, A.H., Jones, W.C., Karakci, A., Keihänen, E., Keskitalo, R., Kiiveri, K., Kim, J., Kisner, T.S., Knox, L., Krachmalnicoff, N., Kunz, M., Kurki-Suonio, H., Lagache, G., Lamarre, J.-M., Lasenby, A., Lattanzi, M., Lawrence, C.R., Le Jeune, M., Lemos, P., Lesgourgues, J., Levrier, F., Lewis, A., Liguori, M., Lilje, P.B., Lilley, M., Lindholm, V., López-Caniego, M., Lubin, P.M., Ma, Y.-Z., Macías-Pérez, J.F., Maggio, G., Maino, D., Mandolesi, N., Mangilli, A., Marcos-Caballero, A., Maris, M., Martin, P.G., Martinelli, M., Martínez-González, E., Matarrese, S., Mauri, N., McEwen, J.D., Meinhold, P.R., Melchiorri, A., Mennella, A., Migliaccio, M., Millea, M., Mitra, S., Miville-Deschénes, M.-A., Molinari, D., Montier, L., Morgante, G., Moss, A., Natoli, P., Nørgaard-Nielsen, H.U., Pagano, L., Paoletti, D., Partridge, B., Patanchon, G., Peiris, H.V., Perrotta, F., Pettorino, V., Piacentini, F., Polastri, L., Polenta, G., Puget, J.-L., Rachen, J.P., Reinecke, M., Remazeilles, M., Renzi, A., Rocha, G., Rosset, C., Roudier, G., Rubiño-Martín, J.A., Ruiz-Granados, B., Salvati, L., Sandri, M., Savelainen, M., Scott, D., Shellard, E.P.S., Sirignano, C., Sirri, G., Spencer, L.D., Sunyaev, R., Suur-Uski, A.-S., Tauber, J.A., Tavagnacco, D., Tenti, M., Toffolatti, L., Tomasi, M., Trombetti, T., Valentiano, L., Valiviita, J., Van Tent, B., Vibert, L., Vielva, P., Villa, F., Vittorio, N., Wandelt, B.D., Wehus, I.K., White, M., White, S.D.M., Zacchei, A., Zonca, A.: Planck 2018 results. VI. Cosmological parameters. *A&A* **641**, 6 (2020) <https://doi.org/10.1051/0004-6361/201833910> [arXiv:1807.06209](https://arxiv.org/abs/1807.06209) [astro-ph.CO]

[54] Behroozi, P.S., Wechsler, R.H., Wu, H.-Y.: The ROCKSTAR Phase-space Temporal Halo Finder and the Velocity Offsets of Cluster Cores. *ApJ* **762**(2), 109 (2013) <https://doi.org/10.1088/0004-637X/762/2/109> [arXiv:1110.4372](https://arxiv.org/abs/1110.4372) [astro-ph.CO]

[55] Behroozi, P.S., Wechsler, R.H., Wu, H.-Y., Busha, M.T., Klypin, A.A., Primack,

J.R.: Gravitationally Consistent Halo Catalogs and Merger Trees for Precision Cosmology. *ApJ* **763**, 18 (2013) <https://doi.org/10.1088/0004-637X/763/1/18> [arXiv:1110.4370](https://arxiv.org/abs/1110.4370) [astro-ph.CO]

[56] Agarwal, B., Khochfar, S., Johnson, J.L., Neistein, E., Dalla Vecchia, C., Livio, M.: Ubiquitous seeding of supermassive black holes by direct collapse. *MNRAS* **425**, 2854–2871 (2012) <https://doi.org/10.1111/j.1365-2966.2012.21651.x> [arXiv:1205.6464](https://arxiv.org/abs/1205.6464) [astro-ph.CO]

[57] Visbal, E., Bryan, G.L., Haiman, Z.: Self-consistent Semianalytic Modeling of Feedback during Primordial Star Formation and Reionization. *ApJ* **897**(1), 95 (2020) <https://doi.org/10.3847/1538-4357/ab994e> [arXiv:2001.11118](https://arxiv.org/abs/2001.11118) [astro-ph.GA]

[58] Kauffmann, G., White, S.D.M., Guiderdoni, B.: The Formation and Evolution of Galaxies Within Merging Dark Matter Haloes. *MNRAS* **264**, 201 (1993)

[59] Hirano, S., Hosokawa, T., Yoshida, N., Omukai, K., Yorke, H.W.: Primordial star formation under the influence of far ultraviolet radiation: 1540 cosmological haloes and the stellar mass distribution. *MNRAS* **448**, 568–587 (2015) <https://doi.org/10.1093/mnras/stv044> [arXiv:1501.01630](https://arxiv.org/abs/1501.01630)

[60] Johnson, J.L., Dalla, V.C., Khochfar, S.: The First Billion Years project: the impact of stellar radiation on the co-evolution of Populations II and III. *MNRAS* **428**, 1857–1872 (2013) <https://doi.org/10.1093/mnras/sts011> [arXiv:1206.5824](https://arxiv.org/abs/1206.5824) [astro-ph.CO]

[61] Scalo, J.: The IMF Revisited: A Case for Variations. In: Gilmore, G., Howell, D. (eds.) *The Stellar Initial Mass Function* (38th Herstmonceux Conference). Astronomical Society of the Pacific Conference Series, vol. 142, p. 201 (1998). <https://doi.org/10.48550/arXiv.astro-ph/9712317>

[62] Barkana, R., Loeb, A.: In the beginning: the first sources of light and the reionization of the universe. *Phys. Rep.* **349**(2), 125–238 (2001) [https://doi.org/10.1016/S0370-1573\(01\)00019-9](https://doi.org/10.1016/S0370-1573(01)00019-9) [arXiv:astro-ph/0010468](https://arxiv.org/abs/astro-ph/0010468) [astro-ph]

[63] Greif, T.H., Bromm, V.: Two populations of metal-free stars in the early Universe. *MNRAS* **373**(1), 128–138 (2006) <https://doi.org/10.1111/j.1365-2966.2006.11017.x> [arXiv:astro-ph/0604367](https://arxiv.org/abs/astro-ph/0604367) [astro-ph]

[64] Kulkarni, M., Visbal, E., Bryan, G.L.: The Critical Dark Matter Halo Mass for Population III Star Formation: Dependence on Lyman-Werner Radiation, Baryon-dark Matter Streaming Velocity, and Redshift. *ApJ* **917**(1), 40 (2021) <https://doi.org/10.3847/1538-4357/ac08a3> [arXiv:2010.04169](https://arxiv.org/abs/2010.04169) [astro-ph.GA]

[65] Chon, S., Hirano, S., Hosokawa, T., Yoshida, N.: Cosmological Simulations of

Early Black Hole Formation: Halo Mergers, Tidal Disruption, and the Conditions for Direct Collapse. *ApJ* **832**, 134 (2016) <https://doi.org/10.3847/0004-637X/832/2/134> arXiv:1603.08923

- [66] Truelove, J.K., Klein, R.I., McKee, C.F., Holliman, J.H. II, Howell, L.H., Greenough, J.A.: The Jeans Condition: A New Constraint on Spatial Resolution in Simulations of Isothermal Self-gravitational Hydrodynamics. *ApJ* **489**, 179 (1997) <https://doi.org/10.1086/310975>
- [67] Matsukoba, R., Tanaka, K.E.I., Omukai, K., Vorobyov, E.I., Hosokawa, T.: Protostellar-disc fragmentation across all metallicities. *MNRAS* **515**(4), 5506–5522 (2022) <https://doi.org/10.1093/mnras/stac2161> arXiv:2206.03497 [astro-ph.GA]
- [68] Shang, C., Bryan, G.L., Haiman, Z.: Supermassive black hole formation by direct collapse: keeping protogalactic gas H_2 free in dark matter haloes with virial temperatures $T_{vir} \gtrsim 10^4$ K. *MNRAS* **402**, 1249–1262 (2010) <https://doi.org/10.1111/j.1365-2966.2009.15960.x> arXiv:0906.4773 [astro-ph.CO]
- [69] Sugimura, K., Omukai, K., Inoue, A.K.: The critical radiation intensity for direct collapse black hole formation: dependence on the radiation spectral shape. *MNRAS* **445**, 544–553 (2014) <https://doi.org/10.1093/mnras/stu1778> arXiv:1407.4039
- [70] Latif, M.A., Bovino, S., Van Borm, C., Grassi, T., Schleicher, D.R.G., Spaans, M.: A UV flux constraint on the formation of direct collapse black holes. *MNRAS* **443**, 1979–1987 (2014) <https://doi.org/10.1093/mnras/stu1230> arXiv:1404.5773
- [71] Regan, J.A., Johansson, P.H., Wise, J.H.: Forming supermassive black hole seeds under the influence of a nearby anisotropic multifrequency source. *MNRAS* **459**, 3377–3394 (2016) <https://doi.org/10.1093/mnras/stw899> arXiv:1511.00696
- [72] Wolcott-Green, J., Haiman, Z., Bryan, G.L.: Photodissociation of H_2 in protogalaxies: modelling self-shielding in three-dimensional simulations. *MNRAS* **418**(2), 838–852 (2011) <https://doi.org/10.1111/j.1365-2966.2011.19538.x> arXiv:1106.3523 [astro-ph.CO]
- [73] Chon, S., Latif, M.A.: The impact of ionizing radiation on the formation of a supermassive star in the early Universe. *MNRAS* **467**, 4293–4303 (2017) <https://doi.org/10.1093/mnras/stx348> arXiv:1611.08594
- [74] Hosokawa, T., Omukai, K.: Evolution of Massive Protostars with High Accretion Rates. *ApJ* **691**(1), 823–846 (2009) <https://doi.org/10.1088/0004-637X/691/1/823> arXiv:0806.4122 [astro-ph]

[75] Haemmerlé, L., Woods, T.E., Klessen, R.S., Heger, A., Whalen, D.J.: The evolution of supermassive Population III stars. *MNRAS* **474**(2), 2757–2773 (2018) <https://doi.org/10.1093/mnras/stx2919> [arXiv:1705.09301](https://arxiv.org/abs/1705.09301) [astro-ph.SR]

[76] Nandal, D., Regan, J.A., Woods, T.E., Farrell, E., Ekström, S., Meynet, G.: Critical accretion rates for rapidly growing massive Population III stars. *A&A* **677**, 155 (2023) <https://doi.org/10.1051/0004-6361/202346938> [arXiv:2306.17223](https://arxiv.org/abs/2306.17223) [astro-ph.SR]

[77] Nandal, D., Chon, S.: Growth of Metal-Enriched Supermassive Stars by Accretion and Collisions. *arXiv e-prints*, 2511–08516 (2025) <https://doi.org/10.48550/arXiv.2511.08516> [arXiv:2511.08516](https://arxiv.org/abs/2511.08516) [astro-ph.SR]

[78] Hosokawa, T., Omukai, K., Yorke, H.W.: Rapidly Accreting Supergiant Protostars: Embryos of Supermassive Black Holes? *ApJ* **756**(1), 93 (2012) <https://doi.org/10.1088/0004-637X/756/1/93> [arXiv:1203.2613](https://arxiv.org/abs/1203.2613) [astro-ph.CO]

[79] Sakurai, Y., Hosokawa, T., Yoshida, N., Yorke, H.W.: Formation of primordial supermassive stars by burst accretion. *MNRAS* **452**, 755–764 (2015) <https://doi.org/10.1093/mnras/stv1346> [arXiv:1505.03954](https://arxiv.org/abs/1505.03954) [astro-ph.SR]

[80] Heger, A., Woosley, S.E.: The Nucleosynthetic Signature of Population III. *ApJ* **567**(1), 532–543 (2002) <https://doi.org/10.1086/338487> [arXiv:astro-ph/0107037](https://arxiv.org/abs/astro-ph/0107037) [astro-ph]

[81] Toyouchi, D., Inayoshi, K., Li, W., Haiman, Z., Kuiper, R.: Radiative feedback on supermassive star formation: the massive end of the Population III initial mass function. *MNRAS* **518**(2), 1601–1616 (2023) <https://doi.org/10.1093/mnras/stac3191> [arXiv:2206.14459](https://arxiv.org/abs/2206.14459) [astro-ph.GA]

[82] Fuller, G.M., Woosley, S.E., Weaver, T.A.: The Evolution of Radiation-dominated Stars. I. Nonrotating Supermassive Stars. *ApJ* **307**, 675 (1986) <https://doi.org/10.1086/164452>

[83] Shibata, M., Shapiro, S.L.: Collapse of a Rotating Supermassive Star to a Supermassive Black Hole: Fully Relativistic Simulations. *ApJ* **572**(1), 39–43 (2002) <https://doi.org/10.1086/341516> [arXiv:astro-ph/0205091](https://arxiv.org/abs/astro-ph/0205091) [astro-ph]

[84] Woods, T.E., Heger, A., Whalen, D.J., Haemmerlé, L., Klessen, R.S.: On the Maximum Mass of Accreting Primordial Supermassive Stars. *ApJ* **842**(1), 6 (2017) <https://doi.org/10.3847/2041-8213/aa7412> [arXiv:1703.07480](https://arxiv.org/abs/1703.07480) [astro-ph.SR]

[85] Uchida, H., Shibata, M., Yoshida, T., Sekiguchi, Y., Umeda, H.: Gravitational collapse of rotating supermassive stars including nuclear burning effects. *Phys. Rev. D* **96**(8), 083016 (2017) <https://doi.org/10.1103/PhysRevD.96.083016> [arXiv:1704.00433](https://arxiv.org/abs/1704.00433) [astro-ph.HE]

[86] Nandal, D., Zwick, L., Whalen, D.J., Mayer, L., Ekström, S., Meynet, G.: The evolution of accreting population III stars at 10^{-6} – 10^3 M_\odot yr $^{-1}$. *A&A* **689**, 351 (2024) <https://doi.org/10.1051/0004-6361/202449562> arXiv:2407.06994 [astro-ph.SR]

[87] Umeda, H., Hosokawa, T., Omukai, K., Yoshida, N.: The Final Fates of Accreting Supermassive Stars. *ApJ* **830**(2), 34 (2016) <https://doi.org/10.3847/2041-8205/830/2/L34> arXiv:1609.04457 [astro-ph.SR]

[88] Sazonov, S.Y., Ostriker, J.P., Sunyaev, R.A.: Quasars: the characteristic spectrum and the induced radiative heating. *MNRAS* **347**(1), 144–156 (2004) <https://doi.org/10.1111/j.1365-2966.2004.07184.x> arXiv:astro-ph/0305233 [astro-ph]

[89] McKinney, J.C., Tchekhovskoy, A., Sadowski, A., Narayan, R.: Three-dimensional general relativistic radiation magnetohydrodynamical simulation of super-Eddington accretion, using a new code HARMRAD with M1 closure. *MNRAS* **441**(4), 3177–3208 (2014) <https://doi.org/10.1093/mnras/stu762> arXiv:1312.6127 [astro-ph.CO]

[90] Inayoshi, K., Haiman, Z., Ostriker, J.P.: Hyper-Eddington accretion flows on to massive black holes. *MNRAS* **459**(4), 3738–3755 (2016) <https://doi.org/10.1093/mnras/stw836> arXiv:1511.02116 [astro-ph.HE]

[91] Watarai, K.-y., Mizuno, T., Mineshige, S.: Slim-Disk Model for Ultraluminous X-Ray Sources. *ApJ* **549**(1), 77–80 (2001) <https://doi.org/10.1086/319125> arXiv:astro-ph/0011434 [astro-ph]

[92] Susa, H.: Smoothed Particle Hydrodynamics Coupled with Radiation Transfer. *PASJ* **58**, 445–460 (2006) <https://doi.org/10.1093/pasj/58.2.445> astro-ph/0601642

[93] Inayoshi, K., Onoue, M., Sugahara, Y., Inoue, A.K., Ho, L.C.: The Age of Discovery with the James Webb Space Telescope: Excavating the Spectral Signatures of the First Massive Black Holes. *ApJ* **931**(2), 25 (2022) <https://doi.org/10.3847/2041-8213/ac6f01> arXiv:2204.09692 [astro-ph.GA]

[94] Bonnor, W.B.: Boyle’s Law and gravitational instability. *MNRAS* **116**, 351 (1956) <https://doi.org/10.1093/mnras/116.3.351>

[95] Ebert, R.: Über die Verdichtung von H I-Gebieten. Mit 5 Textabbildungen. *ZAp* **37**, 217 (1955)

[96] Yoshida, N., Oh, S.P., Kitayama, T., Hernquist, L.: Early Cosmological H II/He III Regions and Their Impact on Second-Generation Star Formation. *ApJ* **663**(2), 687–707 (2007) <https://doi.org/10.1086/518227> arXiv:astro-ph/0610819 [astro-ph]

- [97] Chon, S., Omukai, K.: Supermassive star formation via super competitive accretion in slightly metal-enriched clouds. *MNRAS* **494**(2), 2851–2860 (2020) <https://doi.org/10.1093/mnras/staa863> arXiv:2001.06491 [astro-ph.GA]
- [98] Chon, S., Omukai, K.: Formation of supermassive stars and dense star clusters in metal-poor clouds exposed to strong FUV radiation. *MNRAS* **539**(3), 2561–2582 (2025) <https://doi.org/10.1093/mnras/staf598> arXiv:2412.14900 [astro-ph.GA]
- [99] Yoshida, N., Abel, T., Hernquist, L., Sugiyama, N.: Simulations of Early Structure Formation: Primordial Gas Clouds. *ApJ* **592**(2), 645–663 (2003) <https://doi.org/10.1086/375810> arXiv:astro-ph/0301645 [astro-ph]
- [100] O’Shea, B.W., Norman, M.L.: Population III Star Formation in a Λ CDM Universe. II. Effects of a Photodissociating Background. *ApJ* **673**(1), 14–33 (2008) <https://doi.org/10.1086/524006> arXiv:0706.4416 [astro-ph]